Control Engineering Practice 154 (2025) 106171

Contents lists available at ScienceDirect

Control Engineering Practice

journal homepage: www.elsevier.com/locate/conengprac

3DoF-KF HMPC: A Kalman filter-based Hybrid Model Predictive Control Algorithm for Mixed Logical Dynamical Systems

Owais Khan [a], Mohamed El Mistiri [a], Sarasij Banerjee [a], Eric Hekler [b], Daniel E. Rivera [a,*]

[a] Control Systems Engineering Laboratory, School for Engineering of Matter, Transport, and Energy, Arizona State University, Tempe, AZ 85287, USA
[b] Center for Wireless & Population Health Systems, University of California, San Diego (UCSD), La Jolla, CA 92093, USA

ARTICLE INFO

Keywords:
Model predictive control of hybrid systems
Process control
Robust control
Production planning and control
mHealth
Healthcare decision support
Epidemic control

ABSTRACT

This paper presents the formulation, design procedure, and application of a hybrid model predictive control (HMPC) scheme for hybrid systems that is embedded in a mixed logical dynamical (MLD) framework. The proposed scheme adopts a three degrees-of-freedom (3DoF) tuning method to accomplish precise setpoint tracking and ensure robustness in the face of disturbances (both measured and unmeasured) and uncertainty. Furthermore, the HMPC algorithm employs setpoint and disturbance anticipation to proactively enhance controller performance and potentially reduce control effort. Slack variables in the objective function prevent the mixed-integer quadratic problem from becoming infeasible. The effectiveness of the proposed algorithm is demonstrated through its application in three distinct case studies, which include control of production–inventory systems, time-varying behavioral interventions for physical activity, and management of epidemics/pandemic prevention. These case studies indicate that the HMPC algorithm can effectively manage hybrid dynamics, setpoint tracking and disturbance rejection in diverse and demanding circumstances, while tuned to perform well in the presence of nonlinearity and uncertainty.

1. Introduction

Hybrid systems characterized by the coexistence of continuous dynamics and discrete events form an increasing part of many complex real-world applications. Hybrid systems encompass various sub-classes, each possessing distinct characteristics and requirements; mixed logical dynamical (MLD) systems, which model the dynamics of a hybrid system as a system of linear difference equations subject to inequality constraints involving continuous and discrete variables, stand out as a widely available class of hybrid systems (Bemporad & Morari, 1999; Camacho et al., 2010). By incorporating logical rules and mode transitions, MLD systems provide a precise representation of systems with discrete behaviors and enable the design of mode-dependent control strategies. For MLD systems, a control problem relying on hybrid model predictive control (HMPC) can be solved using mixed-integer linear programming (*milp*) or mixed-integer quadratic programming (*miqp*) methods. Consequently, the controller can systematically optimize control actions over a finite horizon while accounting for system dynamics, diverse constraints, and performance objectives.

In recent years, HMPC has gained increasing attention in the context of MLD systems, finding applications in diverse domains, among these traffic control (Groot et al., 2012), network systems (Gaid et al., 2006), microgrids (Garcia-Torres et al., 2018), traction control (Borrelli et al., 2006), co-generation power plants (Ferrari-Trecate et al., 2004), power electronics (Geyer et al., 2008) and thermal storage in buildings (Berkenkamp & Gwerder, 2014). An emerging application has been to use HMPC for interventions to improve health-related behaviors; these include managing gestational weight gain (Guo et al., 2022), increasing physical activity (El Mistiri et al., 2023; Khan et al., 2022), smoking cessation (Timms et al., 2014), and naltrexone as a treatment for fibromyalgia (Deshpande et al., 2014).

Motivated by the preponderance and complexity of systems with continuous and discrete dynamics, this paper proposes a hybrid model predictive control approach for mixed logical dynamical systems, with emphasis on the large and important sub-class of MLD systems featuring continuous dynamics and hybrid continuous and discrete decisions. The objective is to achieve setpoint tracking and rejection of measured and unmeasured disturbances with an independent and intuitive tuning procedure resulting in satisfactory, robust performance under constraints. The following describes the inspiration for the 3DoF-KF HMPC algorithm and some of its unique properties; these are:

* Corresponding author.
E-mail addresses: okhan5@asu.edu (O. Khan), melmisti@asu.edu (M. El Mistiri), sbaner74@asu.edu (S. Banerjee), ehekler@health.ucsd.edu (E. Hekler), daniel.rivera@asu.edu (D.E. Rivera).

https://doi.org/10.1016/j.conengprac.2024.106171
Received 9 July 2024; Received in revised form 7 November 2024; Accepted 8 November 2024
Available online 21 November 2024

- Discrete controller actions (such as categorical decisions and satisfying "If/Then" conditions) are addressed by using an MLD model for the system under consideration.
- A three-degree-of-freedom (3DoF) formulation based on estimation using two Kalman filters is employed. This formulation enables independent tuning of Type-I and Type-II filters (Morari & Zafiriou, 1989) within the closed-loop system, facilitating direct, individual adjustments for the speed of setpoint tracking as well as the rejection of both measured and unmeasured disturbances. The 3DoF-KF HMPC controller mimics the positive attributes of Internal Model Control (IMC) (Morari & Zafiriou, 1989) while being able to enforce constraints. The combination of intuitive tuning with corresponding robustness proves to be particularly useful.
- The inclusion of slack variables for each output, serving two purposes: penalizing constraint violations and preventing the optimization problem from becoming infeasible. Incorporating slack variables in the objective function with appropriate penalties (in lieu of inequality constraints) allows the optimization problem to remain feasible even if output constraints are not strictly satisfied. This approach enables managing multiple controller objectives using a limited set of manipulated variables.
- The objective function is further enhanced with a terminal cost and a terminal inequality constraint. Terminal inequality constraints ensure feasible predicted trajectories, prevent constraint violations, and guide the system towards desired setpoints for stability, allowing controlled deviation from the setpoint at the final time step. The terminal cost drives convergence by minimizing deviations from the reference trajectory, resulting in accurate tracking. This approach balances the constraint relaxation and optimization objectives, improving the efficiency of the optimization problem.
- The ability to configure the controller for different operation phases of an intervention, when needed. This feature is particularly useful in an application to a behavioral intervention promoting physical activity, where the controller will automatically reconfigure itself to reduce dependence on financial incentives as the participant approaches the goal of 10k steps/day.
- The ability to accomplish both setpoint and disturbance anticipation, enabling proactive adjustment of control actions based on predicted future changes in these variables. The result is improved tracking accuracy, faster response to setpoint transitions, and enhanced disturbance rejection. This feature allows the controller to address requirements preemptively, potentially reducing control effort and avoiding unnecessary adjustments, while ultimately improving overall closed-loop performance.

The paper describes three detailed case studies involving the algorithm that are examined in diverse application settings: (i) inventory and Work-in-Progress (WIP) management in production–inventory systems, (ii) "just-in-time" behavioral interventions for promoting physical activity in sedentary adults, and (iii) epidemic control of a nonlinear Susceptible-Infected-Recovered (SIR) model. The solutions are implemented in MATLAB/Simulink with CPLEX (International Business Machines Corp., 2019) employed to solve the corresponding *miqp* problem. All significant features of the 3DoF-KF HMPC algorithm are collectively illustrated in these case studies, with the results providing compelling evidence for the effectiveness of the proposed strategy in successfully addressing hybrid dynamics, achieving accurate setpoint tracking and disturbance rejection, and attaining robustness under uncertainty.

This paper is structured as follows: Section 2 formulates the problem. Section 3 provides a detailed explanation of the three-degree-of-freedom procedure for setpoint tracking, measured disturbance rejection, and unmeasured disturbance rejection. The formulation of the HMPC scheme for MLD systems is outlined in Section 4. Section 5 provides a comprehensive description of three case studies in which the proposed HMPC algorithm is applied. Concluding remarks and ongoing research activities are presented in Section 6.

2. Problem formulation

2.1. Process model

Consider a hybrid process with dynamics that can be described by the following state-space with MLD model representation (Bemporad & Morari, 1999):

$$x_{k+1} = A_d x_k + B_1 u_k + B_2 \delta_k + B_3 z_k + B_d d_k + B_v v_k \tag{1}$$

$$\eta_k = C x_k + D_v v_k \tag{2}$$

$$y_k = \eta_k + \rho_k \tag{3}$$

$$E_5 \geq E_2 \delta_k - E_4 y_k - E_1 u_k + E_3 z_k + E_d d_k - E_6 u_{k-1} - E_7 y_{k-1} - E_a a_k \tag{4}$$

where $x_k \in \mathbb{R}^{n_x}$ and $u_k \in \mathbb{R}^{n_u}$ represent state and control input with both continuous and binary entries, respectively. $\eta_k \in \mathbb{R}^{n_y}$ is the process noise-free output, $y_k \in \mathbb{R}^{n_y}$ represents the measurable process output, $d_k \in \mathbb{R}^{n_{dist}}$ represents measured disturbance, v_k is the unmeasured disturbance, and ρ_k represents measurement noise. The measurement noise at each output is assumed to be white noise with a diagonal covariance matrix: $E\{\rho\rho^T\} = \Gamma = \text{diag}\{\sigma_1, \ldots, \sigma_{n_y}\}$, $\sigma_j \geq 0$. $\delta_k \in \{0,1\}^{n_d}$ and $z_k \in \mathbb{R}^{n_z}$ correspond to auxiliary variables (binary and categorical discrete respectively) that serve to incorporate logical decisions through (4). The dimensionality of the auxiliary variables is determined by the number of linear constraints specified in (4), which are directly related to the distinct features of logical decisions (Bemporad & Morari, 1999). The variable a_k functions as an additional signal within the propositional logic, allowing the controller to behave according to user-specified requirements.

The system being analyzed is open-loop stable, with v_k as a random signal that follows the model:

$$\zeta_{k+1} = A_w \zeta_k + B_w w_k \tag{5}$$

$$v_k = C_w \zeta_k \tag{6}$$

The matrix A_w possesses eigenvalues that are contained within the unit disk, while w_k represents integrated white noise. The unmeasured disturbance vector v_k is assumed to comprise uncorrelated components, leading to the conditions $B_w = C_w = \mathcal{I}$, where $\mathcal{I}$ refers to the identity matrix with suitable dimensions. Moreover, A_w is defined as $A_w = \text{diag}\{\Lambda_1, \ldots, \Lambda_{n_y}\}$, where the entries of A_w are 0 for disturbances with a single integrator and 1 for disturbances with double integrator (Morari & Zafiriou, 1989).

By applying the difference operator $\Delta = 1 - q^{-1}$ to Eqs. (1)–(4) and (5), an extended state-space model is established in the following manner:

$$X_{k+1} = \mathcal{A} X_k + \mathcal{B}_1 \Delta u_k + \mathcal{B}_2 \Delta \delta_k + \mathcal{B}_3 \Delta z_k + \mathcal{B}_d \Delta d_k + \mathcal{B}_w \Delta w_k \tag{7}$$

$$y_k = \mathcal{C} X_k + \rho_k \tag{8}$$

where

$$X_k = \begin{bmatrix} \Delta x_k \\ \Delta \zeta_k \\ \eta_k \end{bmatrix}, \quad \mathcal{A} = \begin{bmatrix} A & B_v C_w & 0 \\ 0 & A_w & 0 \\ CA & CB_v C_w + D_v C_w A_w & \mathcal{I} \end{bmatrix}, \quad \mathcal{C} = \begin{bmatrix} 0 & 0 & \mathcal{I} \end{bmatrix}$$

$$\mathcal{B}_i = \begin{bmatrix} B_i \\ 0 \\ CB_i \end{bmatrix}, \quad \mathcal{B}_w = \begin{bmatrix} 0 \\ B_w \\ D_v C_w B_w \end{bmatrix}, \quad i = 1, 2, 3, d$$

The variable Δw_k is considered to be a white noise with a diagonal covariance matrix.

$$E\{\Delta w_k \Delta w_k^T\} = \mathcal{W} = \text{diag}\{\omega_1, \omega_2, \ldots, \omega_{n_y}\}, \ \omega_j \geq 0$$

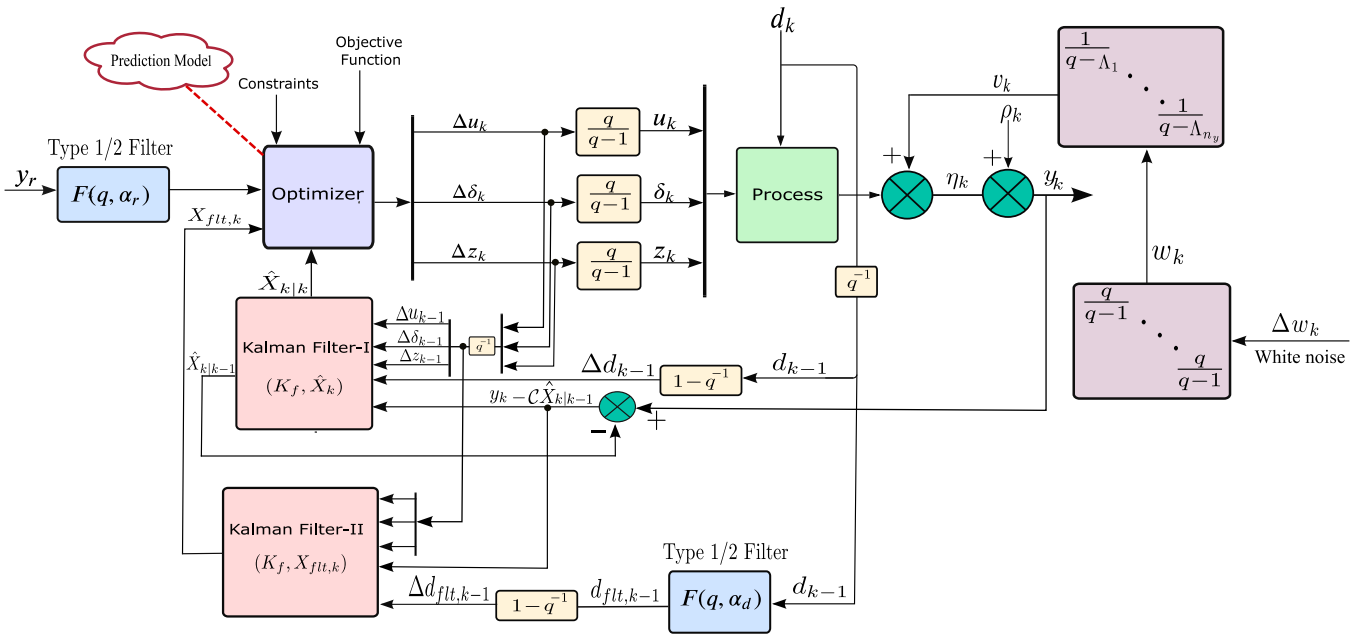

Fig. 1. Schematic diagram depicting the application of a proposed Kalman filter-based HMPC scheme to a process. The scheme aims to achieve setpoint tracking while effectively accounting for both measured and unmeasured disturbances. The controller utilizes filtered signals obtained by filtering the measured disturbances and setpoint as its inputs. Kalman Filter-I is associated with (25)–(26), while Kalman Filter-II is associated with (27)–(28).

2.2. HMPC problem

Taking into consideration the insights from Bemporad and Morari (1999), a quadratic cost function is employed:

$$\begin{aligned} J_k \triangleq & \sum_{j=1}^{p-1} \left\| (y_{k+j} - y_{r,k+j}) \right\|^2_{W_y} + \sum_{i=0}^{m-1} \left\| (\Delta u_{k+i}) \right\|^2_{W_{du}} \\ & + \sum_{i=0}^{m-1} \left\| (u_{k+i} - u_{r,k+i}) \right\|^2_{W_u} + \sum_{j=1}^{p} \left\| (\delta_{k+j} - \delta_{r,k+j}) \right\|^2_{W_d} \\ & + \sum_{j=1}^{p} \left\| (z_{k+j} - z_{r,k+j}) \right\|^2_{W_z} + \left\| (y_{k+p} - y_{r,k+p}) \right\|^2_{W_{yt}} \end{aligned} \tag{9}$$

y_r represents the unfiltered setpoint, p stands for the prediction horizon, m for the control horizon, and $W_* > 0$ stands for weight matrix corresponding to the relevant process variable. The respective reference trajectory is denoted by $(\cdot)_r$, The vector 2-norm weighted by the matrix W is denoted as $\|(\cdot)\|_{W*} \triangleq \sqrt{(\cdot)^T W_* (\cdot)}$. Mathematically, the optimization problem can be represented as follows:

$$\min_{u_{k+i},\ \delta_{k+j},\ z_{k+j},\ \psi_{k+j}} J_k + \sum_{j=1}^{p} \left\| (\psi_{k+j}) \right\|^2_{W_s} \tag{10}$$

subject to mixed integer constraints in (4) and

$$y_{\min} - \psi_{k+j} \leq \quad y_{k+j} \quad \leq y_{\max} + \psi_{k+j} \tag{11}$$

$$u_{\min} \leq \quad u_{k+i} \quad \leq u_{\max} \tag{12}$$

$$\Delta u_{\min} \leq \quad \Delta u_{k+i} \leq \Delta u_{\max} \tag{13}$$

$$\psi_{k+j} \geq 0 \tag{14}$$

$$\forall i = 0, 1, \ldots, m-1, \quad \forall j = 1, 2, \ldots, p$$

$\psi \in \mathbb{R}^{n_y}$ denotes the slack variables and $W_s > 0$ represents the corresponding penalty weight matrix. The choice of W_s is user-defined, and its value specifies the extent of constraint enforcement. As W_s increases, the importance of constraint enforcement also increases. If W_s is sufficiently large ($W_s \to \infty$), "soft" constraints effectively behave as "hard" constraints. To achieve a higher level of flexibility, a separate slack variable for each output is used over the prediction horizon, thereby increasing the degrees of freedom. At the final step of the prediction horizon, terminal inequality constraints are added to the optimization problem. These constraints allow for a controlled deviation from the setpoint at the final time step and define an acceptable region around the setpoint. Doing so they influence system behavior over the long term while simultaneously ensuring feasibility and stability. $u_{\min}$, $u_{\max}$, $\Delta u_{\min}$, $\Delta u_{\max}$, $y_{\min}$, and $y_{\max}$ are lower and upper bounds on inputs, move sizes, and outputs, respectively.

The goal is to develop an HMPC decision algorithm for the extended model expressed in Eqs. (7)–(8) that can minimize the objective function expressed in (9), reliably track the target setpoint in the presence of measured and unmeasured disturbances, and satisfy constraints in (11)–(14). This can be accomplished by employing Kalman filters to accurately estimate the state X of the extended model, as discussed in the next section. Fig. 1 presents a block diagram that depicts the underlying philosophy of our proposed HMPC scheme for the constrained process. The optimizer is used to find a sequence of decision variables that can effectively minimize the objective function stated in Eq. (10) while satisfying the constraints expressed in Eqs. (11)–(14). Using first-order low-pass filters, the white noise signal (w_k) becomes a stochastic, autocorrelated disturbance (v_k).

3. Three-degree-of-freedom procedure

The MPC formulation employed in this study relies on a 3DoF tuning mechanism that enables the performance requirements for setpoint tracking, unmeasured disturbance rejection, and anticipated measured disturbance rejection to be separately adjusted. Each degree of freedom is characterized by a speed-of-response parameter whose selection is simpler and more intuitive than specifying weights (e.g. move suppression) as done in traditional MPC formulations. This procedure is described in the ensuing subsections:

3.1. Reference trajectory/setpoint tracking

A filter is used to generate the filtered setpoint $y_{r,flt}$ from the unfiltered setpoint y_r (Khan et al., 2022), i.e., $\forall j = 1, \ldots, n_y$

$$\frac{y_{r,flt,k+i}}{y_{r,k+i}} = f(q, \alpha_r^j), \quad \forall i = 1, \ldots, p \tag{15}$$

where $f(q,\alpha_r^j)$ is a Type-I discrete-time filter for the j-th reference as given in (Morari & Zafiriou, 1989).

$$f(q,\alpha_r^j)=\frac{(1-\alpha_r^j)q}{q-\alpha_r^j},\quad 0\le\alpha_r^j<1,\ \ \forall j=1,\dots,n_y \tag{16}$$

The setpoint tracking speed can be adjusted by selecting time constants τ_r^j for setpoint tracking, which correspond to unique values of α_r^j for each output j. Mathematically, the relationship between the desired closed-loop time constant (τ_r) and the parameter (α_r) is described by the following equation:

$$\tau_r^j=-\frac{T_s}{\ln(\alpha_r^j)}\Rightarrow\alpha_r^j=e^{-T_s/\tau_r^j} \tag{17}$$

where T_s is the sampling time and $\ln(\alpha_r)$ denotes the natural logarithm of α_r. Lower values of α_r^j result in faster setpoint tracking of output j. The variables u_r, δ_r, and z_r are assumed to be constant at their respective predefined target values over the prediction horizon.

3.2. Measured disturbance rejection

The proposed formulation utilizes externally generated forecasts for both unfiltered and filtered measured disturbances. These forecasts serve as anticipated signals, which are subsequently supplied to the control algorithm. The measured disturbance signals are filtered as follows:

$$\frac{d_{flt,k+i}}{d_{k+i}}=f(q,\alpha_d^j),\ \forall j=1,\dots,n_{dist}$$
$$\forall i=0,1,\dots,p-1 \tag{18}$$

where $f(q,\alpha_d^j)$ can be either a Type-I (asymptotic step) filter or a Type-II (asymptotic ramp) filter depending on the nature of the system dynamics. A Type-II filter will be utilized if an asymptotically ramp disturbance exists; otherwise, a Type-I filter will be employed. For the system to be Type n_f, the filter has to satisfy

$$\text{Type } n_f:\ \frac{d^k}{dq^k}(1-f(q,\alpha_d^j))\Big|_{q=1}=0 \tag{19}$$

For a Type I system, (19) is satisfied with $f(q,\alpha_d^j)=1$, $\forall j=1,\dots,n_{dist}$, and the filter

$$f(q,\alpha_d^j)=\frac{(1-\alpha_d^j)q}{q-\alpha_d^j},\quad 0\le\alpha_d^j<1 \tag{20}$$

clearly meets that requirement. For $n_f\ge 2$, the filter given in (20) is not sufficient. In this case, the following filter structure is examined (Morari & Zafiriou, 1989).

$$f(q,\alpha_d^j)=(\beta_0+\beta_1q^{-1}+\cdots+\beta_\omega q^{-\omega})\times\frac{(1-\alpha_d^j)q}{q-\alpha_d^j} \tag{21}$$

where the coefficients $\beta_0,\beta_1,\dots,\beta_\omega$ are chosen such that $f(1,\alpha_d^j)$ satisfies (19) for a user-specified value of α_d^j (also within the range [0 1). For a Type-II system with $n_f=2$, it is important to choose $\omega\ge 2$ to avoid the trivial solution $f(q,\alpha_d^j)=1$. The minimum norm solution for $n_f=2$ and $\omega\ge 2$, is found to be

$$\beta_k=\frac{-6k\alpha_d^j}{(1-\alpha_d^j)\omega(\omega+1)(2\omega+1)}, \tag{22}$$

$$\beta_0=1-(\beta_1+\cdots+\beta_\omega),\quad\forall k=1,2,\dots,\omega \tag{23}$$

The speed at which measured disturbances are rejected can be independently adjusted by employing a filter $f(q,\alpha_d^j)$ for each individual measured disturbance signal. The value of α_d^j can be tuned by regulating the desired closed-loop time constant τ_d^j for each measured disturbance j and is defined by the equation:

$$\tau_d^j=-\frac{T_s}{\ln(\alpha_d^j)}\Rightarrow\alpha_d^j=e^{-T_s/\tau_d^j} \tag{24}$$

The values of τ_d for each disturbance influence the speed of measured disturbance rejection. When the value of α_d^j is decreased, the speed of disturbance rejection will increase.

3.3. Unmeasured disturbance rejection

Given that the state X_k in Eqs. (7)–(8) cannot be directly measured, it is necessary to employ a filter for estimating X_k. To ensure precise future predictions of the output y_k and enable true 3DoF, a two-step procedure for estimating the augmented state X_k is presented. In the first step, the state $\hat{X}_k$ of the state X_k is estimated by utilizing the following filter structure, which takes into account both unfiltered measured disturbance d_k and unmeasured disturbances.

$$\hat{X}_{k|k-1}=\mathcal{A}\hat{X}_{k-1|k-1}+\mathcal{B}_1\Delta u_{k-1}+\mathcal{B}_2\Delta\delta_{k-1}+\mathcal{B}_3\Delta z_{k-1}+\mathcal{B}_d\Delta d_{k-1} \tag{25}$$

$$\hat{X}_{k|k}=\hat{X}_{k|k-1}+\mathcal{K}_f(y_k-\mathcal{C}\hat{X}_{k|k-1}) \tag{26}$$

$\hat{X}_{k|k-1}$ is the value of $\hat{X}$ at time instant k estimated at time instant $k-1$. Given that the unfiltered measured disturbance d_k is utilized in Eqs. (25), the correction term in Eq. (26) specifically represents the impact of unmeasured disturbances. The speed and nature of rejecting these unmeasured disturbances are shaped by the selection of the gain matrix $\mathcal{K}_f$. Finally, in the estimation of an augmented system state, both the filtered measured disturbance signal d_{flt} and the contribution arising from the unmeasured disturbance are taken into account. This contribution is obtained as the prediction error resulting from Eqs. (25)–(26).

$$X_{flt,k|k-1}=\mathcal{A}X_{flt,k-1|k-1}+\mathcal{B}_1\Delta u_{k-1}+\mathcal{B}_2\Delta\delta_{k-1}+\mathcal{B}_3\Delta z_{k-1}$$
$$+\mathcal{B}_d\Delta d_{flt,k-1} \tag{27}$$

$$X_{flt,k|k}=X_{flt,k|k-1}+\mathcal{K}_f(y_k-\mathcal{C}\hat{X}_{k|k-1}) \tag{28}$$

$X_{flt,k|k-1}$ is the value of X_{flt} at time instant k estimated at time instant $k-1$. The terms in Eq. (28) (except for the last term) represent the impact of the filtered measured disturbances. On the other hand, the correction term in (26) represents the effect of the unmeasured disturbances. Therefore, the variable $X_{flt,k}$ considers both the filtered measured disturbances and the unmeasured disturbances. This filter structure ensures that the tuning for measured disturbances (denoted by α_d^j) does not impact the rejection of unmeasured disturbances. Conversely, adjusting the gain matrix $\mathcal{K}_f$ does not influence the rejection speed of the measured disturbances. In other words, the measured disturbances and unmeasured disturbances are decoupled within this filter design.

The optimal value of the gain matrix $\mathcal{K}_f$ can be computed by solving the algebraic Riccati equation (Maciejowski, 2002)

$$\mathcal{P}_\infty=\mathcal{A}\mathcal{P}_\infty\mathcal{A}^T-\mathcal{A}\mathcal{P}_\infty\mathcal{C}^T\left[\mathcal{C}\mathcal{P}_\infty\mathcal{C}^T+\Gamma\right]^{-1}\mathcal{C}\mathcal{P}_\infty\mathcal{A}^T+\mathcal{B}_w\mathcal{W}\mathcal{B}_w^T \tag{29}$$

where $\mathcal{P}_\infty$ is the only positive-definite solution, and from which the stationary gain matrix $\mathcal{K}_f$ can be computed as:

$$\mathcal{K}_f=\mathcal{P}_\infty\mathcal{C}^T\left[\mathcal{C}\mathcal{P}_\infty\mathcal{C}^T+\Gamma\right]^{-1} \tag{30}$$

Nevertheless, doing so necessitates estimating covariance matrices for unmeasured disturbances, which may not be precisely known. Instead, the parameterization approach described in Lee et al. (1994) is adopted; it provides the user with the flexibility to customize the speed of unmeasured disturbance rejection for each output channel. For an asymptotically stable plant, the algebraic Riccati Eq. (29) associated with the model (7)–(8) has a solution.

$$\mathcal{P}=\begin{bmatrix}0&0&0\\0&\mathcal{P}_{22}&\mathcal{P}_{23}\\0&\mathcal{P}_{23}^T&\mathcal{P}_{33}\end{bmatrix} \tag{31}$$

where the dimensions of the blocks correspond to the dimensions of the vectors x, ζ, and y. Consequently, the Kalman filter gain matrix is given by

$$\mathcal{K}_f=\begin{bmatrix}0\\\mathcal{P}_{23}\\\mathcal{P}_{33}\end{bmatrix}\left[\mathcal{P}_{33}+\Gamma\right]^{-1} \tag{32}$$

Furthermore, since A_w and $\mathcal{W}$ are both diagonal, the blocks $\mathcal{P}_{23}$ and $\mathcal{P}_{33}$ are both diagonal (and square). Consequently, $\mathcal{K}_f$ has the form

$$\mathcal{K}_f = \begin{bmatrix} 0 & F_w^T & F_y^T \end{bmatrix}^T \tag{33}$$

where

$$F_w = \text{diag}\left\{ f_w^1, \quad \cdots, \quad f_w^{n_y} \right\}$$
$$F_y = \text{diag}\left\{ f_y^1, \quad \cdots, \quad f_y^{n_y} \right\}$$
$$f_w^j = \frac{(f_y^j)^2}{1 + \Lambda_j - \Lambda_j f_y^j}, \ \forall j = 1, \ldots, n_y$$

and

$$f_y^j \to 0 \ \text{ as } \ \omega_j/\sigma_j \to 0 \tag{34}$$
$$f_y^j \to 1 \ \text{ as } \ \omega_j/\sigma_j \to \infty \tag{35}$$

The tuning parameter f_y^j, which ranges from 0 to 1 for all values of ω_j/σ_j, can be adjusted by regulating the time constant τ_u for each output channel. Therefore, by appropriately tuning τ_u, the impact of unmeasured disturbances can be effectively mitigated. The relationship between the desired closed-loop time constant (τ_u) and the parameter (f_y) follows the equation:

$$\tau_u^j = -\frac{T_s}{\ln(f_y^j - 1)} \Rightarrow f_y^j = 1 - e^{-T_s/\tau_u^j} \tag{36}$$

The tuning parameter f_y^j directly affects the speed at which unmeasured disturbances are rejected. As f_y^j approaches zero, the state estimator progressively pays less attention to the correction of prediction errors. In such cases, the control solution primarily relies on the deterministic model (25) and the feedforward anticipation signal. Conversely, as f_y^j approaches 1, the state estimator aims to compensate for all prediction errors, leading to an aggressive controller behavior. By adjusting the value of f_y^j instead of the variances ω_j and σ_j, users have a direct and intuitive means (in comparison to adjusting move suppression in conventional MPC formulations) to influence unmeasured disturbance rejection and impact the robustness of the control system (Lee & Yu, 1994).

Remark 1. It needs mentioning that the MLD model in Eqs. (1)–(4) is capable of accommodating discrete outputs. However, in this paper all output signals are assumed to be continuous. In Eqs. (32) and (33), the filter gain matrix $\mathcal{K}_f$ is parameterized in such a way that the elements corresponding to Δx_k (which may include both continuous and discrete system states) are set to 0. As a result, unmeasured disturbances do not affect the original system states x_k, but only the outputs y_k are adjusted to compensate for the cumulative impact of all disturbances in the process. This characteristic enables the proposed MPC formulation to achieve offset-free responses when dealing with asymptotic step or ramp disturbances on the outputs, depending on whether $A_w = 0$ or $A_w = \mathcal{I}$ is chosen, respectively. To achieve this, it is necessary to measure all controlled outputs. Additionally, the controller effectively rejects asymptotic step or ramp disturbances by utilizing the integral action derived from the augmented model in the difference form with $A_w = 0$ or $A_w = \mathcal{I}$, respectively.

3.4. Robustness considerations

A key factor in tuning MPC controllers is accounting for the trade-off between performance and robustness (Garriga & Soroush, 2010). In the three-degree-of-freedom formulation, plant-model mismatch is treated as an unmeasured disturbance, and the controller's sensitivity to model uncertainty is determined by the tuning of the unmeasured disturbance mode via f_y^j (Schwartz & Rivera, 2010; Schwartz et al., 2006). For linear continuous (non-hybrid) systems, Lee and Yu (1994) describes a robustness analysis of the filter from Eqs. (25)–(35) under unconstrained conditions. In particular, they present the sensitivity and complementary sensitivity functions for the closed-loop system across a range of values for f_y^j and Λ_i, and how formal robustness guarantees can be achieved by utilizing the concept of the Structured Singular Value (Zhou et al., 1996). Formally testing the robustness of MPC is considerably more challenging in the constrained case with discrete decision variables, although some intuitive methods can be considered (Rossiter, 2003). Within the scope of this paper, it is not possible to present a formal proof illustrating the effect of these tuning and disturbance parameters on the robustness of a constrained hybrid system. Considering the direct connection between the value of f_y^j and the nominal closed-loop bandwidth, it is expected that as f_y^j approaches 0, increasing robustness will come at the cost of performance. Robustness considerations will form part of the discussion of the case studies presented in Section 5.

4. Formulation of HMPC for MLD systems

In this section, a formulation of the HMPC strategy for MLD systems is introduced. To predict the future values of the output variable y_k, Eqs. (25)–(28) are utilized and propagated forward for p steps into the future. At each step, it is assumed that the future error correction term $(y_{k+1} - C\hat{X}_{k+1|k})$ is equal to zero, as it is not available at the current sampling instant k. This assumption is reasonable and can be shown to be optimal (Maciejowski, 2002). Additionally, it is essential to take into account the forecasted values of unfiltered and filtered measured disturbances, denoted as Δd_{k+l} and $\Delta d_{flt,k+l}$ respectively, where $l = 1, 2, \ldots, p$. Therefore, by considering these assumptions, the following output prediction equation for the objective function (expressed in (10)) is formulated by propagating (27)–(28) for p steps into the future.

$$\mathcal{Y}_{flt,k+1} = \Phi X_{flt,k} + \mathcal{H}_1 \mathcal{U}_k + \mathcal{H}_2 \bar{\delta}_k + \mathcal{H}_3 \mathcal{Z}_k + \mathcal{H}_d \mathcal{D}_{flt,k} - \mathcal{H}_{11} u_{k-1} - \mathcal{H}_{21} \delta_{k-1} - \mathcal{H}_{31} z_{k-1} - \mathcal{H}_{d1} d_{flt,k-1} \tag{37}$$

Moreover, an output prediction equation for the constraints (expressed in (4), (11)–(14)) is formulated by propagating (25)–(26) for p steps into the future.

$$\hat{\mathcal{Y}}_{k+1} = \Phi \hat{X}_k + \mathcal{H}_1 \mathcal{U}_k + \mathcal{H}_2 \bar{\delta}_k + \mathcal{H}_3 \mathcal{Z}_k + \mathcal{H}_d \mathcal{D}_k - \mathcal{H}_{11} u_{k-1} - \mathcal{H}_{21} \delta_{k-1} - \mathcal{H}_{31} z_{k-1} - \mathcal{H}_{d1} d_{k-1} \tag{38}$$

where $\mathcal{H}_1, \Psi_{k+1}$ are given in Box I.

$$\mathcal{Y}_{flt,k+1} = \begin{bmatrix} y_{flt,k+1} \\ y_{flt,k+2} \\ \vdots \\ y_{flt,k+p} \end{bmatrix}, \quad \hat{\mathcal{Y}}_{k+1} = \begin{bmatrix} \hat{y}_{k+1} \\ \hat{y}_{k+2} \\ \vdots \\ \hat{y}_{k+p} \end{bmatrix}, \quad \Phi = \begin{bmatrix} C\mathcal{A} \\ \vdots \\ C\mathcal{A}^p \end{bmatrix}, \quad \bar{\delta}_k = \begin{bmatrix} \delta_k \\ \delta_{k+1} \\ \vdots \\ \delta_{k+p-1} \end{bmatrix}$$

$$\mathcal{Z}_k = \begin{bmatrix} z_k \\ z_{k+1} \\ \vdots \\ z_{k+p-1} \end{bmatrix}, \quad \mathcal{D}_k = \begin{bmatrix} d_k \\ d_{k+1} \\ \vdots \\ d_{k+p-1} \end{bmatrix}, \quad \mathcal{D}_{flt,k} = \begin{bmatrix} d_{flt,k} \\ d_{flt,k+1} \\ \vdots \\ d_{flt,k+p-1} \end{bmatrix}$$

$$\mathcal{U}_k = \begin{bmatrix} u_k \\ u_{k+1} \\ \vdots \\ u_{k+m-1} \end{bmatrix}, \quad H_{i1} = \begin{bmatrix} C\mathcal{B}_i \\ C\mathcal{A}\mathcal{B}_i \\ \vdots \\ C\mathcal{A}^{p-1}\mathcal{B}_i \end{bmatrix}, \quad i = 1, 2, 3, d$$

Similarly, the inequality expressed in (4) is propagated for p steps into the future. Hence, it follows that

$$\bar{E}_5 \geq \bar{E}_2 \bar{\delta}_k + \bar{E}_3 \mathcal{Z}_k + \bar{E}_1 \mathcal{U}_k + \bar{E}_4 \hat{\mathcal{Y}}_k + \bar{E}_d \mathcal{D}_k + \bar{E}_6 u_{k-1} + \bar{E}_7 y_{k-1} - \bar{E}_a \bar{a}_k \tag{39}$$

where

$$\bar{E}_i = \text{diag}\{E_i, \ldots, E_i\}, \ i = 2, \ 3, \ d. \ a$$
$$\bar{E}_j = \begin{bmatrix} -E_j & 0 & \cdots 0 \end{bmatrix}^T, \ j = 6, 7$$

$$\mathcal{H}_1 = \begin{bmatrix} \mathcal{C}\mathcal{B}_1 & 0 & \cdots & 0 & 0 \\ \mathcal{C}\mathcal{A}\mathcal{B}_1 - \mathcal{C}\mathcal{B}_1 & \mathcal{C}\mathcal{B}_1 & \cdots & 0 & 0 \\ \mathcal{C}\mathcal{A}^2\mathcal{B}_1 - \mathcal{C}\mathcal{A}\mathcal{B}_1 & \mathcal{C}\mathcal{A}\mathcal{B}_1 - \mathcal{C}\mathcal{B}_1 & \ddots & \vdots & \vdots \\ \vdots & \vdots & \ddots & \mathcal{C}\mathcal{B}_1 & \vdots \\ \mathcal{C}\mathcal{A}^{m-1}\mathcal{B}_1 - \mathcal{C}\mathcal{A}^{m-2}\mathcal{B}_1 & \mathcal{C}\mathcal{A}^{m-2}\mathcal{B}_1 - \mathcal{C}\mathcal{A}^{m-1}\mathcal{B}_1 & \cdots & \mathcal{C}\mathcal{A}\mathcal{B}_1 - \mathcal{C}\mathcal{B}_1 & \mathcal{C}\mathcal{B}_1 \\ \mathcal{C}\mathcal{A}^{m}\mathcal{B}_1 - \mathcal{C}\mathcal{A}^{m-1}\mathcal{B}_1 & \mathcal{C}\mathcal{A}^{m-1}\mathcal{B}_1 - \mathcal{C}\mathcal{A}^{m-2}\mathcal{B}_1 & \cdots & \mathcal{C}\mathcal{A}^2\mathcal{B}_1 - \mathcal{C}\mathcal{A}\mathcal{B}_1 & \mathcal{C}\mathcal{A}\mathcal{B}_1 \\ \vdots & \vdots & \vdots & \vdots & \vdots \\ \mathcal{C}\mathcal{A}^{p-1}\mathcal{B}_1 - \mathcal{C}\mathcal{A}^{p-2}\mathcal{B}_1 & \mathcal{C}\mathcal{A}^{p-2}\mathcal{B}_1 - \mathcal{C}\mathcal{A}^{p-1}\mathcal{B}_1 & \cdots & \mathcal{C}\mathcal{A}^{p-m+1}\mathcal{B}_1 - \mathcal{C}\mathcal{A}^{p-m}\mathcal{B}_1 & \mathcal{C}\mathcal{A}^{p-m}\mathcal{B}_1 \end{bmatrix}$$

$$\Psi_{k+1} = \begin{bmatrix} \psi_{k+1} \\ \psi_{k+2} \\ \vdots \\ \psi_{k+p} \end{bmatrix}, \quad \mathcal{H}_i = \begin{bmatrix} \mathcal{C}\mathcal{B}_i & 0 & \cdots & 0 & 0 \\ \mathcal{C}\mathcal{A}\mathcal{B}_i - \mathcal{C}\mathcal{B}_i & \mathcal{C}\mathcal{B}_i & \cdots & 0 & 0 \\ \mathcal{C}\mathcal{A}^2\mathcal{B}_i - \mathcal{C}\mathcal{A}\mathcal{B}_i & \mathcal{C}\mathcal{A}\mathcal{B}_i - \mathcal{C}\mathcal{B}_i & \cdots & \vdots & \vdots \\ \vdots & \vdots & \ddots & \vdots & \vdots \\ \mathcal{C}\mathcal{A}^{p-1}\mathcal{B}_i - \mathcal{C}\mathcal{A}^{p-2}\mathcal{B}_i & \mathcal{C}\mathcal{A}^{p-2}\mathcal{B}_i - \mathcal{C}\mathcal{A}^{p-3}\mathcal{B}_i & \cdots & \mathcal{C}\mathcal{A}\mathcal{B}_i - \mathcal{C}\mathcal{B}_i & \mathcal{C}\mathcal{B}_i \end{bmatrix}, \quad i = 2,\ 3,\ d$$

Box I.

$$\bar{E}_1 = \begin{bmatrix} -E_1 & 0 & \cdots & 0 \\ -E_6 & \ddots & \ddots & 0 \\ 0 & \ddots & \ddots & \vdots \\ 0 & \ddots & -E_6 & -E_1 \\ 0 & \ddots & 0 & -E_6 - E_1 \\ \vdots & \vdots & 0 & \vdots \\ 0 & \cdots & \cdots & -E_6 - E_1 \end{bmatrix}, \quad \bar{a}_k = \begin{bmatrix} a_k \\ a_{k+1} \\ \vdots \\ a_{k+p-1} \end{bmatrix}$$

$$\bar{E}_4 = \begin{bmatrix} -E_4 & 0 & \cdots & 0 \\ -E_7 & -E_4 & \ddots & 0 \\ 0 & \ddots & \ddots & \vdots \\ \vdots & \ddots & -E_7 & -E_4 \end{bmatrix}, \quad \bar{E}_5 = \begin{bmatrix} E_5 \\ E_5 \\ \vdots \\ E_5 \end{bmatrix}$$

Eq. (39) can be further simplified by substituting $\hat{\mathcal{Y}}_k$ from (38) and rewriting it as,

$$\begin{aligned} \mathcal{E}_5 \geq\ & \mathcal{E}_2\bar{\delta}_k + \mathcal{E}_3\mathcal{Z}_k + \mathcal{E}_1\mathcal{U}_k + \mathcal{E}_d D_k + \mathcal{E}_4\hat{X}_k - \mathcal{E}_{41}u_{k-1} - \mathcal{E}_{42}\delta_{k-1} \\ & - \mathcal{E}_{43}z_{k-1} - \mathcal{E}_{4d}d_{k-1} + \mathcal{E}_6 u_{k-1} + \mathcal{E}_7 y_{k-1} - \mathcal{E}_a\bar{a}_k \end{aligned} \tag{40}$$

where

$$\mathcal{E}_i = \left(\bar{E}_i + \bar{E}_4\bar{\mathcal{H}}_i\right), \quad \mathcal{E}_4 = \bar{E}_4\bar{\Phi}, \quad \mathcal{E}_j = \bar{E}_j, \quad j = 5,\ 6,\ 7,\ a$$

$$\mathcal{E}_{4i} = \bar{E}_4\bar{\mathcal{H}}_{i1}, \ i = 1,\ 2,\ 3,\ d$$

$$\bar{\Phi} = \begin{bmatrix} C \\ \Phi(1:(p-1)n_y, :) \end{bmatrix}, \quad \bar{\mathcal{H}}_i = \begin{bmatrix} [0]_{n_y} \\ \mathcal{H}_i(1:(p-1)n_y, :) \end{bmatrix}$$

$$i = 1, 2, 3, d, 11, 21, 31, d1$$

The HMPC problem stated in (9)–(14) can now be reformulated in vector form by utilizing (37) into the objective function and (38) into the constraints.

$$\begin{aligned} \min_{\substack{\mathcal{U}_k, \bar{\delta}_k, \\ \mathcal{Z}_k, \Psi_{k+1}}} J_k \triangleq\ & \left\|(\mathcal{Y}_{flt,k+1} - \mathcal{Y}_{r,flt,k+1})\right\|^2_{\widehat{W}_y} + \left\|(\mathcal{U}_k - \mathcal{U}_{r,k})\right\|^2_{\widehat{W}_u} + \\ & \left\|(\mathcal{Z}_k - \mathcal{Z}_{r,k})\right\|^2_{\widehat{W}_z} + \left\|(R_u\mathcal{U}_k - R_{u0}u_{k-1})\right\|^2_{\widehat{W}_{du}} + \left\|\Psi_{k+1}\right\|^2_{\widehat{W}_s} \end{aligned} \tag{41}$$

subject to mixed integer constraints according to (40) and

$$\mathcal{Y}_{\min} - \Psi_{k+1} \leq \hat{\mathcal{Y}}_{k+1} \leq \mathcal{Y}_{\max} + \Psi_{k+1} \tag{42}$$

$$\mathcal{U}_{\min} \leq \mathcal{U}_k \leq \mathcal{U}_{\max} \tag{43}$$

$$\Delta\mathcal{U}_{\min} \leq \Delta\mathcal{U}_k \leq \Delta\mathcal{U}_{\max} \tag{44}$$

$$\Psi_{k+1} \geq 0 \tag{45}$$

where $\widehat{W}_* = \mathrm{diag}(W_*)$, and

$$R_{u0} = \begin{bmatrix} \mathcal{I} \\ 0 \\ \vdots \\ 0 \end{bmatrix}, \quad R_u = \begin{bmatrix} \mathcal{I} & 0 & \cdots & 0 & 0 \\ -\mathcal{I} & \mathcal{I} & \cdots & 0 & 0 \\ 0 & -\mathcal{I} & \ddots & \vdots & \vdots \\ \vdots & \vdots & \ddots & \ddots & \vdots \\ 0 & 0 & \cdots & -\mathcal{I} & \mathcal{I} \end{bmatrix}$$

The variables $\mathcal{Y}_{r,flt}$, $\mathcal{U}_r$, $\bar{\delta}_r$, and $\mathcal{Z}_r$ represent the reference vectors for the outputs, inputs, auxiliary binary variables, and auxiliary continuous variables respectively, as provided below:

$$\mathcal{Y}_{r,flt,k+1} = \begin{bmatrix} y^T_{r,flt,k+1} & y^T_{r,flt,k+2} & \cdots & y^T_{r,flt,k+p} \end{bmatrix}^T \tag{46}$$

$$\mathcal{U}_{r,k} = \begin{bmatrix} u^T_{r,k} & u^T_{r,k+1} & \cdots & u^T_{r,k+m-1} \end{bmatrix}^T \tag{47}$$

$$\bar{\delta}_{r,k} = \begin{bmatrix} \delta^T_{r,k} & \delta^T_{r,k+1} & \cdots & \delta^T_{r,k+p-1} \end{bmatrix}^T \tag{48}$$

$$\mathcal{Z}_{r,k} = \begin{bmatrix} z^T_{r,k} & z^T_{r,k+1} & \cdots & z^T_{r,k+p-1} \end{bmatrix}^T \tag{49}$$

As the constant terms do not impact the optimization problem and the optimal solution, they are excluded from the objective function. Next, by substituting $\mathcal{Y}_{flt,k+1}$ and $\hat{\mathcal{Y}}_{k+1}$ as expressed in Eqs. (37)–(38) into (41)–(42), and performing straightforward computations, the following *miqp* problem is obtained.

$$\min_{\xi_k} J_k \triangleq \frac{1}{2}\xi_k^T\mathcal{H}\xi_k + \mathcal{G}^T\xi_k \tag{50}$$

$$\tilde{\mathcal{S}}\xi_k \leq \mathcal{M} \tag{51}$$

Here $\xi_k = [\mathcal{U}_k^T, \bar{\delta}_k^T, \mathcal{Z}_k^T, {\Psi_{k+1}}^T]^T$ represents the decision variables for the optimization problem per (50) and (51). To ensure convexity in the *miqp* optimization problem, the Hessian matrix $\mathcal{H}$ representing the quadratic terms must satisfy the conditions of being symmetric and positive definite (or semi-definite). Additionally, the gradient vector $\mathcal{G}$ accounts for the linear terms. The coefficient matrices $\tilde{\mathcal{S}}$ and $\mathcal{M}$ are employed to express the constraints.

$$\mathcal{H} = 2\mathcal{Q}, \quad \mathcal{G} = 2\begin{bmatrix} g_1^T \\ g_2^T \\ g_3^T \\ 0 \end{bmatrix}, \quad \tilde{\mathcal{S}} = \begin{bmatrix} \tilde{\mathcal{S}}_1 \\ \tilde{\mathcal{S}}_2 \\ \tilde{\mathcal{S}}_3 \\ \tilde{\mathcal{S}}_4 \end{bmatrix}, \quad \mathcal{M} = \begin{bmatrix} b_1 \\ b_2 \\ b_3 \\ b_4 \\ b_5 \\ 0 \end{bmatrix}$$

The coefficient matrices can be found in Appendix. For the design and implementation of the proposed scheme, a detailed step-by-step procedure is provided and summarized in Algorithm 1.

4.1. Stability and convergence

The nominal stability and convergence properties of HMPC using MLD models are discussed in Theorem 1. The *miqp* optimization problem defined in (50)–(51) incorporates the prominent features of a synthesis approach of HMPC, like robust stability and feasibility.

Algorithm 1 3DoF-KF HMPC Algorithm

1. Specify the design parameters, i.e. p, m, τ_r^i (or α_r^i), τ_d^j (or α_d^j), τ_u^i (or f_y^i), $1 \le i \le n_y$, $1 \le j \le n_{dist}$, and the corresponding weight matrices and limits that are defined in (9)–(14).
2. Obtain the measurements y_k, u_{k-1} and d_k.
3. Initialize Kalman Filter-I at $k = 0$ to estimate the augmented state using unfiltered measured disturbances Δd_{k-1} according to equations (25)–(26), assuming steady-state conditions ($\Delta\delta_{k-1} = 0$, $\Delta z_{k-1} = 0$). The filter gain $\mathcal{K}_f$ can be calculated using (33).
4. Initialize Kalman Filter-II at $k = 0$ using the estimated augmented state obtained in step 3 and the filtered measured disturbances $\Delta d_{flt,k-1}$ to ensure accurate 3DoF estimation and to decouple the effects of unmeasured and filtered measured disturbances, as shown in (27)–(28).
5. Solve the *miqp* problem expressed in (50)–(51) to obtain a sequence of control actions and other decision variables, namely $\mathcal{U}_k$, $\bar{\delta}_k$, and $\bar{z}_k$. Using the receding horizon principle, implement the first control move $u_{k|k}$ to the process model to obtain new measurements.
6. Set $k = k + 1$, wait until the next sampling time, and return to step 3, utilizing the estimated augmented state, unfiltered and filtered measured disturbances, and decision variables obtained in the previous iteration.

Theorem 1. *For the system under consideration subjected to constraints (4) and (11)–(14), the miqp optimization problem expressed in (50)–(51) is solved at each sampling instant k. At each sampling instant k, assume the existence of an initial state x_0 such that the corresponding miqp problem (50)–(51) is feasible. Then, for any given weights $W_y \ge 0$, $W_{yt} \ge 0$, $W_{du} > 0$, $W_u > 0$, $W_d \ge 0$, and $W_z \ge 0$:*

1. *The miqp problem (50)–(51) is also feasible for the sampling instant $k + 1$.*
2. *The closed-loop dynamics of HMPC converge asymptotically as follows:*
   - $\lim_{k\to\infty} y_k = y_{r,flt}$, *indicating convergence of the output y_k to the filtered reference trajectory $y_{r,flt}$*
   - $\lim_{k\to\infty} \|\Delta u_k\|_{W_{du}} = 0$, *denoting convergence of incremental inputs Δu_k*
   - $\lim_{k\to\infty} u_k = u_r$, *representing convergence of the manipulated variables u_k to u_r*
   - $\lim_{k\to\infty} \|\delta_k - \delta_r\|_{W_d} = 0$, *representing convergence of the binary auxiliary variables δ_k to δ_r*
   - $\lim_{k\to\infty} \|z_k - z_r\|_{W_z} = 0$, *representing convergence of the continuous auxiliary variables z_k to z_r*

   Moreover, the closed-loop system satisfies constraints (4) and (11)–(14) at each sampling instant $k \ge 0$.

Proof. The proof is an extension of the one provided in Bemporad and Morari (1999), and can be shown utilizing Lyapunov theory and following straightforward computations. □

Remark 2. The HMPC formulation in this work employs distinct prediction equations, (37) for the objective function and (38) for constraints, to balance optimality and robustness. For the objective function expressed in (10), Kalman Filter-II (described in (27)–(28)) with filtered measured disturbances is used, providing accurate future state predictions and ensuring true 3DoF control. For constraints expressed in (4), (11)–(14), Kalman Filter-I (described in (25)–(26)) with unfiltered measured disturbances (that the real plant experiences) is employed, reflecting the actual system state more accurately for robust constraint satisfaction, capturing rapid variations more precisely. This choice allows solutions closer to actual system constraints and ensures robust constraint satisfaction by accurately reflecting real-time physical limitations.

This dual choice of prediction equations theoretically results in a slightly relaxed miqp optimization problem compared to using (37) for both objective function and constraints. It offers superior performance by balancing optimized control actions with robust constraint handling, capturing rapid variations more accurately while avoiding overly conservative solutions that may occur with filtered measured disturbance based prediction Eq. (37) for both objective and constraints.

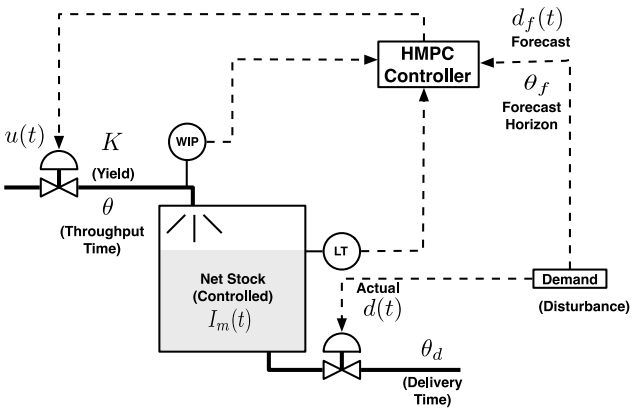

Fig. 2. Schematic diagram for a classical production–inventory system that considers how starts $u(t)$ can be adjusted to maintain inventory I_m(t) at setpoint while satisfying capacity constraints on Work-in-Progress (WIP).

Table 1
Control design parameters for the production–inventory problem.

Parameter	Value	Parameter	Value
p	30 days	m	20 days
α_d (Faster tuning)	$[0\ \ 0]^T$	F_y (Faster tuning)	diag{1, 1}
α_d (Slower tuning)	$[0.9\ \ 0]^T$	F_y (Slower tuning)	diag{0.3, 0.3}
α_r (Faster tuning)	$[0\ \ 0]^T$	α_r (Slower tuning)	$[0.9\ \ 0]^T$
u_{min}	0	u_{max}	100
Δu_{min}	$-\infty$	Δu_{max}	∞
y_{max} (For Fig. 4)	$[800,\ 150]^T$	y_{min} (For Fig. 4)	$[0,\ 0]^T$
y_{max} (For Fig. 3)	$[\infty,\ \ \infty]^T$	y_{min} (For Fig. 3)	$[-\infty,\ -\infty]^T$
W_u, W_{du}	0, 0.4	W_y, W_{yt}	diag{1, 0}

5. Case studies

The effectiveness and versatility of the algorithm is demonstrated in a series of industrially-relevant case studies; these include:

1. Control of production–inventory systems, meaningful in manufacturing and enterprise systems,
2. Development of personalized interventions for physical activity, a relevant problem to mHealth and population health, and
3. Control of an SIR epidemic model, a topic relevant to pandemic prevention.

These are described in the ensuing subsections.

5.1. Application to production inventory

The production–inventory system is a widely studied problem with numerous applications in enterprises (Nandola & Rivera, 2013). Fig. 2 depicts a schematic of a production–inventory system incorporating both feedback and feedforward control decisions. This system can be effectively modeled using a fluid analogy. In this analogy, the production

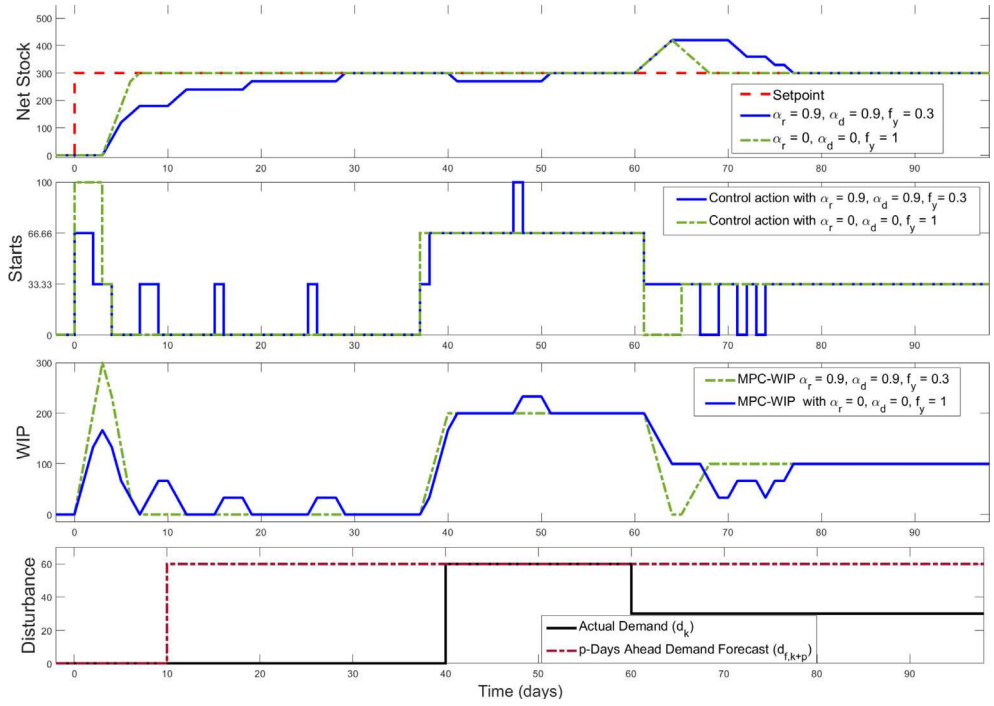

Fig. 3. Simulation results demonstrating the application of proposed 3DoF HMPC algorithm to the classical production–inventory model, showcasing both fast and slow tuning of the filters within the algorithm. In the bottom panel, two disturbances are depicted: one measured disturbance occurring at day 40 and an unmeasured disturbance occurring at day 10.

node is represented as a pipe with a throughput time denoted by θ days and yield denoted by K. The inventory is analogous to material or fluid stored in a tank. Additionally, the delivery process from the warehouse is represented as a pipe with a transportation time of θ_d days. By applying the principle of mass conservation, a differential equation is derived that relates the net stock (material inventory denoted as I_m) to factory starts (input pipe flow denoted as $u(t)$) and consumer demand (output tank flow denoted as $d(t)$), while also establishing a differential equation that describes the relationship between WIP and factory starts:

$$\frac{d\,I_m(t)}{dt} = Ku(t-\theta) - d(t) \tag{52}$$

$$\frac{d\,WIP(t)}{dt} = u(t) - u(t-\theta) \tag{53}$$

where I_m is the controlled variable, WIP is the Work-In-Progress that refers to materials that are being assembled but not yet finished product, and $u(t)$ is the manipulated variable. Customer demand $d(t)$ is composed of the sum of the forecasted demand ($d_f(t)$, known θ_f days ahead of time) and unforecasted demand $d_{uf}(t)$ as shown below:

$$d(t) = d_f(t-\theta_f) + d_{uf}(t) \tag{54}$$

In discrete time, for daily sampling, the dynamics of this system are governed by the equations

$$I_{m,k+1} = I_{m,k} + Ku_{k-\theta} - d_k \tag{55}$$

$$WIP_{k+1} = WIP_k + u_k - u_{k-\theta} \tag{56}$$

The primary objective of this system is to meet customer demand d_k while simultaneously maintaining the net stock inventory at a predetermined target level. This involves sensibly adjusting the factory starts and incorporating feedforward compensation based on the forecasted demand $d_{f,k}$. The control system strives to achieve a proper balance between production output and demand, ensuring that the inventory remains within the specified target range. In the specific scenario considered in this case study, the manipulated input u_k is limited to four specific values: 0, 33.33, 66.66, and 100. As a result, the plant described by Eq. (55) falls into a category of a hybrid system characterized by a discrete-level input u_k and a continuous output y_k. The system can be effectively represented and modeled using the MLD framework, as outlined in (1)–(4). To account for the discrete nature of the input, binary auxiliary variables (δ_1, δ_2, δ_3, δ_4) and continuous auxiliary variables (z_1, z_2, z_3, z_4) are introduced, and their relationships are defined as follows:

$$\delta_{1,k} = 1 \Leftrightarrow z_{1,k} = 0 \tag{57}$$

$$\delta_{2,k} = 1 \Leftrightarrow z_{2,k} = 33.33 \tag{58}$$

$$\delta_{3,k} = 1 \Leftrightarrow z_{3,k} = 66.66 \tag{59}$$

$$\delta_{4,k} = 1 \Leftrightarrow z_{4,k} = 100 \tag{60}$$

$$\sum_{i=1}^{n_{cd}} \delta_{i,k} = 1, \quad u_k = \sum_{i=1}^{n_{cd}} z_{i,k} \tag{61}$$

where n_{cd} denotes the number of categorical decisions. The symbol "⇔" should be read as *if and only if* (*e.g.* $\delta_{1,k} = 1$ *if and only if* $z_{1,k} = 0$ else 0 or vice versa). The conditions specified in (57)–(61) ensure that the input u_k can only assume one of four specific values at any given instant. The logical implication (⇔) in (57)–(59) can be represented as linear inequality constraints using propositional logic equivalence (Williams, 1993), which can then be transformed into a matrix representation as shown in (4). This results in an MLD model for the production–inventory problem mentioned earlier. The MLD model can be utilized to formulate an HMPC problem in the form of (50)–(51). For this particular case, certain parameter values are assumed: a sampling time of $T_s = 1$ day, θ_f and p set to 30 days, a system gain of K set to 0.9, and a throughput time of θ equal to 3 days.

Fig. 3 depicts the effect of manipulating the tuning parameters α_r, α_d, and f_y on the nominal speed of response and the robustness of the algorithm. As mentioned earlier, both the speed of setpoint tracking and the speed of measured disturbance rejection vary inversely with the values of α_r and α_d, respectively. Additionally, the speed of unmeasured disturbance rejection is directly influenced by the value of f_y. To initiate the analysis, a step change with a magnitude of 300 is introduced in the setpoint. The solid line in the figure corresponds to the controller's performance when the 3DoF tuning parameters $\alpha_r = 0.9$,

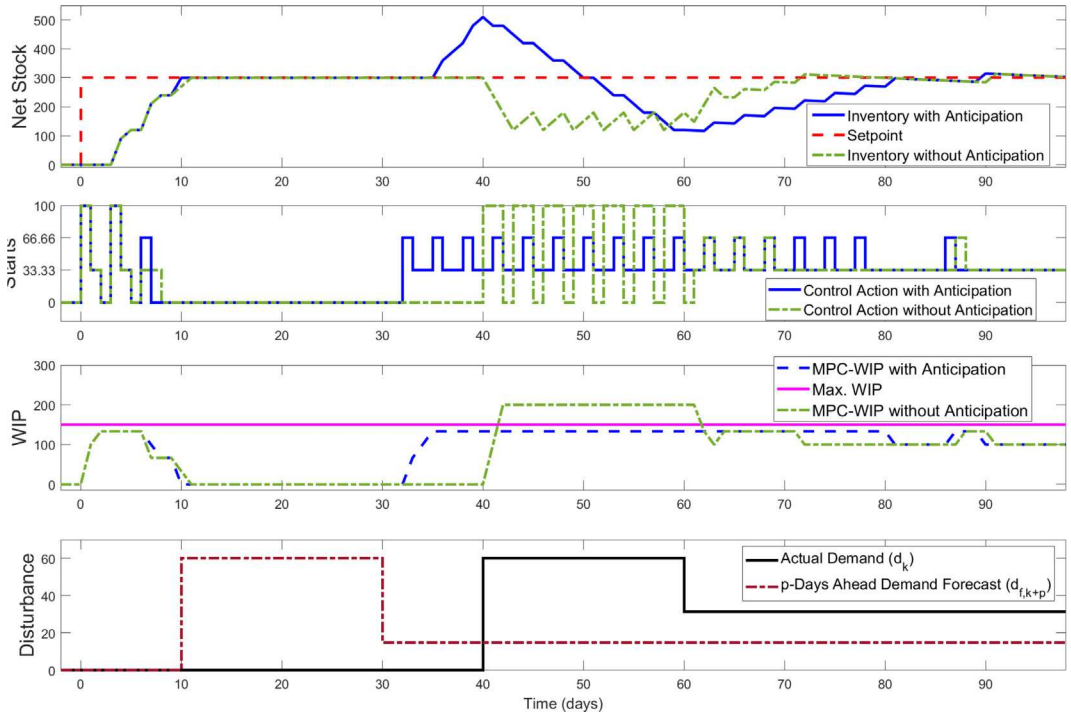

Fig. 4. Simulation results demonstrating the effectiveness of disturbance anticipation in the proposed HMPC algorithm. The figure further showcases the impact of including a slack variable in the objective function, ensuring the feasibility of the optimization problem. The second-to-last panel of the figure illustrates the response of the Work in Progress (WIP) variable, which meet the WIP constraint due to utilizing anticipation feature whereas violates the WIP constraint in the absence of anticipation feature. The proposed optimization problem is feasible for both the cases: with anticipation and without anticipation, due to the inclusion of slack, the algorithm avoids becoming stuck and successfully maintains system stability despite the constraint violation.

$\alpha_d = 0.9$, and $f_y = 0.3$ are employed, while the dashed lines represent the controller's performance using the parameters $\alpha_r = \alpha_d = 0$ and $f_y = 1$. It is evident from the graph that the system achieves quicker setpoint tracking when α_r is set to 0.9 in comparison to when it is set to 0.

On day 40, a step change in the actual demand d_k with a magnitude of 60 is introduced. This change is accurately forecasted without any error, so d_k equals the forecasted demand $d_{f,k}$, which remains at 60 until day 60. When $\alpha_d = 0$, the controller promptly detects the demand change and takes immediate feedforward action to maintain the inventory at the setpoint without any deviation (shown as the dashed line). However, when $\alpha_d = 0.9$, the production rate slows down, resulting in a decrease in inventory (shown as the solid line).

On day 61, demand experiences a sudden decrease from 60 to 30. This change introduces a negative bias of 30 units in the forecast, representing an unmeasured disturbance ($d_{uf,k} = d_k - d_{f,k} = -30$). In this scenario, the controller initiates feedback action; however, it takes some time for the controller to detect the decrease in demand, leading to the inventory exceeding the setpoint. Nevertheless, through continuous control action, the system gradually settles at the setpoint. Comparing the values of f_y, a faster rejection of unmeasured disturbances is achieved when $f_y = 1$ in contrast to $f_y = 0.3$. The simulation results effectively illustrate how the adjustable parameters α_r, α_d, and f_y have a discernible impact on the closed-loop response of the production–inventory system. By adjusting these parameters, users can attain desired levels of performance and robustness.

Fig. 4 provides visual evidence supporting the effectiveness of incorporating disturbance anticipation and slack into the HMPC algorithm. Tuning parameters of the controller can be found in Table 1. Here the solid line in the figure corresponds to the controller's performance in the presence of disturbance anticipation, while the dashed lines represent the controller's performance without anticipation. The results presented in both cases demonstrate the controller's performance under the influence of faster 3DoF tuning parameters, specifically $\alpha_r = \alpha_d = 0$, and $f_y = 1$. On day 40, there is a step change in the actual demand d_k with a magnitude of 60. This change is accurately forecasted without any error, so d_k equals the forecasted demand $d_{f,k}$, which remains at 60 until day 60. On day 61, the demand suddenly decreases from 60 to 30. This change introduces a negative bias of 15 units in the forecast, representing an unmeasured disturbance ($d_{uf,k} = d_k - d_{f,k} = -15$). As is evident from Fig. 4, the controller (with anticipation) proactively builds inventory prior to the occurrence of the actual demand d_k, and thus prevents violations of the WIP constraint. By doing so, the algorithm avoids the need to use slack. Without the anticipation feature, the controller lacks the ability to forecast future demand; as a result, when the demand enters at day 40, the inventory levels start to decline gradually, as indicated by the dashed line in the top panel of the graph. However, during this period, the controller takes advantage of slack, which allows for violations of the WIP constraint. By utilizing this slack allowance with a weight of $W_s = \text{diag}\{1,\ 100\}$, the system gains flexibility to gradually increase the inventory level, reaching the desired setpoint and avoiding further violations of the WIP constraint.

5.2. Application to Just Walk, a behavioral intervention for increasing physical activity

Just Walk is an adaptive behavioral intervention developed at Arizona State University, specifically tailored for overweight and sedentary individuals (Hekler et al., 2018; Phatak et al., 2018). The primary objective of this intervention is to create dynamic models of participants using system identification techniques, with the ultimate goal of motivating sedentary individuals to walk 10,000 steps a day. To achieve this, participants are assigned daily step goals and provided with incentives in the form of expected points. When participants meet their daily goals, these expected points are converted into granted points. As a result, participants can redeem the awarded points for rewards such as gift cards.

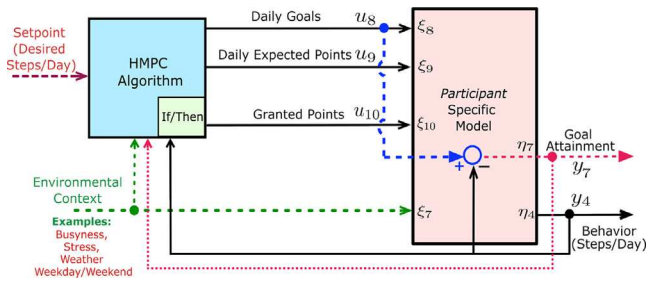

Fig. 5. Schematic of a closed-loop behavioral intervention based on a participant model from *Just Walk*.

In this study, an objective evaluation of the hybrid model predictive control approach for MLD systems is conducted. The approach utilizes a dynamical model estimated from data obtained during the *Just Walk* intervention. The closed-loop intervention comprises two distinct stages. The first stage, known as the *initiation* phase, focuses on guiding individuals towards a healthier state by setting daily "ambitious but doable" step goals and providing rewards when the goals are met. The second stage, referred to as the *maintenance* phase, involves eliminating rewards as individuals come close to the 10,000 step/day goal. The transition from initiation to maintenance phases (and possible return to initiation, if necessary) is managed by the control algorithm.

5.2.1. Intervention design and development

In this intervention, individual performance is evaluated by taking into account the following signals (also known as intervention constructs):

- Daily Goals (u_8): An external cue that is used to indicate the target number of steps to be achieved on a daily basis, such as 10,000 steps per day.
- Daily Expected Points (u_9): A predetermined number of points announced on a daily basis for the individuals who successfully meet their daily goals. This point allocation serves as an outcome expectancy for reinforcement, offering motivation and incentivizing individuals to achieve their objectives.
- Granted Points (u_{10}): The number of points awarded to individuals upon achieving the daily goals, which is equivalent to the daily expected points. This allocation of points is accomplished through an "If/Then" block.
- Behavior (y_4): The total number of steps walked at the end of the day.
- Goal Attainment ($y_7 = y_4 - u_8$): the difference between daily goals and behavior, reflecting a participant's ability to attain their goal.

In this case study, goal attainment is treated as an output signal, subject to constraints. Details of the output constructs of the *Just Walk* identification model (depicted in Fig. 5) based on Social Cognitive Theory (SCT) can be found in the work by Martín et al. (2020). For the *Just Walk* dynamic model, the input and output vectors are

$$u = \begin{bmatrix} u_8 & u_9 & u_{10} \end{bmatrix}^T, \quad y = \begin{bmatrix} y_4 & y_7 \end{bmatrix}^T \tag{62}$$
$$n_{uc} = 1, \; n_{ud} = 2, \; n_y = 2$$

The environmental context signals, *Temperature* and *Weekday/Weekend*, are considered as measured disturbances. Unmeasured disturbances (e.g., a family member's illness or an unexpected party invitation) are presumed to follow a Gaussian distribution and impact only the daily steps taken, rather than influencing the system states (i.e., $B_v = 0$, $D_v = I$).

5.2.2. Problem-specific constraints

Values of the intervention components are determined by continuous daily goals u_8 and a discrete set of expected points $u_{9,k}$, where $u_{9,k} \in U_9 = \{0, 50, 100, 150, 20\}$. As a result, the auxiliary variables can be defined as follows:

$$\delta_{j,k} = 1 \Leftrightarrow z_{j,k} = 50 \times j, \quad \forall j = 0, \dots, n_{cd} \tag{63}$$

This condition is enforced by

$$z_{j,k} = 50 \times j \times \delta_{j,k}, \quad \forall j = 0, \dots, n_{cd} \tag{64}$$

Here $n_{cd} = 4$. To enforce the exclusive assignment of a single value to u_9 at each sampling instant k, it is essential to integrate the following constraints into the proposed HMPC scheme.

$$\sum_{j=0}^{n_{cd}} \delta_{j,k} = 1, \quad u_{9,k} = \sum_{j=0}^{n_{cd}} z_{j,k} \tag{65}$$

The impact of all entries for a specific day can only be assessed based on the outputs recorded after midnight, as the step count for that day is logged until 11:59 PM and resets to zero at the start of the next day. Consequently, the output measurements are adjusted to align temporally with their corresponding inputs from that day. The propositional logic discussed here is a key component of the HMPC formulation and can be represented by the E matrices defined in (4). It is vital to address output measurement limitations and ensure that *Expected Points* convert to *Granted Points* at the beginning of the next day. To indicate whether the goal has been met, the auxiliary variable δ_{gs} is used, which assesses if the steps taken on the previous day $(k-1)$ meet or exceed the daily target goal (steps). This concept can be further elucidated by examining the underlying logic.

$$\delta_{gs,k} = 1 \Leftrightarrow y_{4,k-1} \geq u_{8,k-1} \tag{66}$$

The technique known as big-M reformulation is used to convert logical constraints into a set of linear conditions that maintain the same feasible set (Martín et al., 2016). To determine the value of δ_{gs}, the following constraints are taken into consideration:

$$y_{4,k-1} - u_{8,k-1} \leq \delta_{gs,k} \, [y_4^{max} - u_8^{min}] \tag{67}$$

$$y_{4,k-1} - u_{8,k-1} \geq [1 - \delta_{gs,k}] \, [y_4^{min} - u_8^{max}] \tag{68}$$

To represent the granted points, auxiliary variable $z_{gs} = u_{9,k-1}\delta_{gs,k}$ is introduced, where $u_{10,k} = z_{gs,k}$. At the start of each day, goal attainment is checked. If the goal has been met (i.e., goal attainment is greater than or equal to zero), the granted points ($u_{10,k}$) for the current day are set equal to the expected points ($u_{9,k-1}$) that were announced on the previous day. This can be expressed mathematically as:

$$u_{9,k-1} - z_{gs,k} \leq [1 - \delta_{gs,k}][u_9^{max} - u_{10}^{min}] \tag{69}$$

$$u_{9,k-1} - z_{gs,k} \geq [1 - \delta_{gs,k}][u_9^{min} - u_{10}^{max}] \tag{70}$$

If the goals are not achieved, no points are given that day ($u_{10} = 0$)

$$z_{gs,k} \geq \delta_{gs,k} u_{10}^{min}, \quad z_{gs,k} \leq \delta_{gs,k} u_{10}^{max} \tag{71}$$

The constraints described by (66)–(71) are incorporated in (4) by defining the values for matrices in (4) through the HYSDEL Toolbox (Torrisi & Bemporad, 2004).

5.2.3. Maintenance phase

A maintenance phase is incorporated into the intervention to avoid financial dependency. During this phase, financial incentives for participants are reduced, encouraging them to sustain healthy behavior without relying on monetary rewards.

The maintenance phase initiates when the intervention target of 10,000 steps/day is achieved for at least $n_s - 2$ days out of the last n_s days. In this phase, a participant's daily step count must remain within a specified range of the intervention target, defined by a tolerance value *tol*. The HMPC algorithm is reconfigured to sustain desired behavior with minimal reliance on financial rewards, reducing dependency on

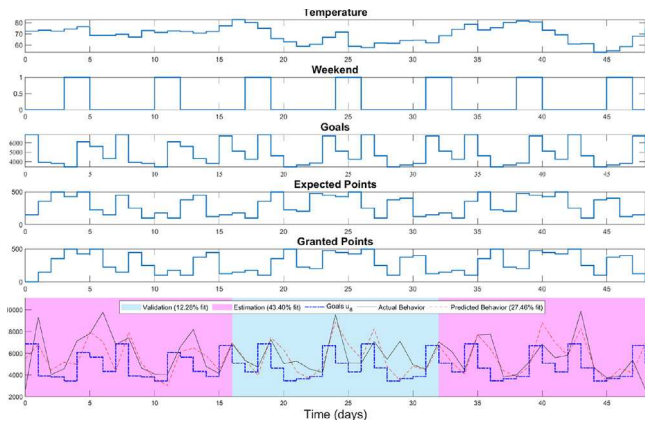

Fig. 6. Time series plot displaying results from ARX modeling for three (of five) multisine cycles for a representative *Just Walk* participant. Five input sequences corresponding to measured disturbances (*Temperature* and *Weekend*) and manipulated variables (*Goals*, *Expected Points* and *Granted Points*) are shown from top. The bottom plot displays predicted *Behavior* (estimated from an ARX model), actual *Behavior* and daily *Goals* (all in steps/day). Estimation and validation data regions are highlighted in magenta and cyan, respectively. The overall NRMSE fit is 27.46% (with 43.40% fit for estimation and 12.28% fit for validation). The ARX model is estimated using regularized least-squares regression with a model order of $n_a = 2$, $n_b = n_k = [1\ 1\ 1\ 1\ 1]$; regularization parameters are $\lambda = 10^2$ and $\mathcal{R} = 1$.

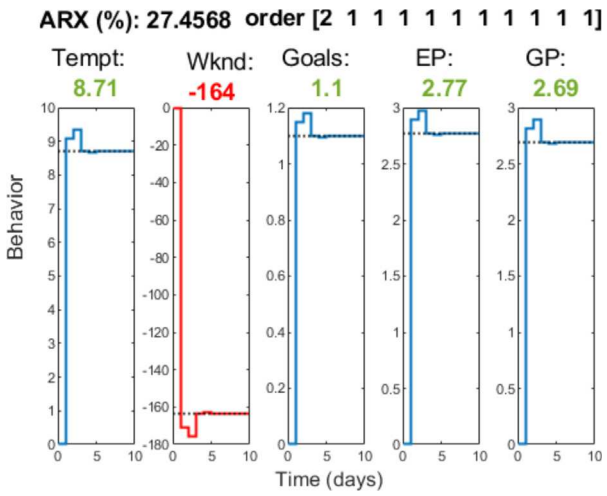

Fig. 7. Step responses of regularized ARX identified model for the five inputs: Temperature, Weekday/Weekend, Goals, Expected Points (EP), and Granted Points (GP) along with their DC gains.

monetary incentives. Furthermore, the HMPC must be able to reintroduce rewards (expected points) in the event of significant behavioral relapses. This reconfiguration is achieved by modifying the penalty weights in the objective function, reflecting the unique considerations of each intervention phase. To implement this criterion effectively, a new auxiliary logical variable ϵ_k is introduced. (Note that this variable is not included in the general HMPC formulation as outlined in (1)–(4)).

$$\epsilon_{k-i} = 1 \leftrightarrow |y_{4,k-i} - y_{4,r}| \leq tol, \quad \forall i = 0, \dots, n_s - 1 \tag{72}$$

Hence, the maintenance phase is activated at sampling instant k if the following condition holds.

$$\sum_{i=0}^{n_s-1} \epsilon_{k-i} \geq n_s - 2 \tag{73}$$

During the maintenance phase, the controller is reconfigured to reduce the use of expected points (u_9). For target inputs represented as $u_r = [u_{8,r} \quad u_{9,r} \quad u_{10,r}]^T$, an appropriate value for $u_{9,r}$ is selected (e.g., $u_{9,r} = 0$ points/day), while simultaneously adjusting the input weight matrix to $W_u = \text{diag}\{0, w_9, 0\}$. The value of w_9 influences the expected performance of setpoint tracking relative to meeting the input target. If, at any given sampling instant k, the condition specified in (73) is not satisfied (indicating a potential relapse), the controller reactivates the initiation phase. This reactivation introduces rewards (expected points) to the participant to restore the desired behavior level, effectively bringing the participant back into the maintenance phase.

5.2.4. Simulation results

Experimental data from a representative *Just Walk* participant (Fig. 6) was utilized to estimate a personalized dynamic model via system identification, using the procedure described in El Mistiri et al. (2023). ARX estimation with regularization is employed for one participant, with the model generated by estimating over the inputs *Temperature*, *Weekday/Weekend*, *Goals*, *Expected Points* (EP) and *Granted Points* (GP); step responses are shown in Fig. 7. In accordance with the input signal cycles, the data were split into five sub-experiments (each sub-experiment representing one 16-day multisine cycle), allowing for testing various combinations of estimation and validation data and reducing bias from any "novelty effects" at the start of the intervention. For estimation, the first, third, and fifth sub-experiments were employed, while validation was carried out using the second and fourth sub-experiments.

Fig. 8 showcases the application of the proposed HMPC scheme to the representative identified model of *Just Walk* intervention. The tuning parameters for the controller can be found in Table 2. The results demonstrate the effectiveness of the HMPC algorithm in delivering a personalized behavioral intervention based on the individual model. HMPC effectively delivers a personalized behavioral intervention by setting progressively increasing, "ambitious but attainable" targets for the daily step count. Initially, during the approximately 31-days initiation phase, reasonable goals and expected points are used to motivate the participant and provide rewards upon achieving daily goals. As can be seen in Fig. 8, the controller successfully awards granted points with a unit delay when the goals are achieved, abiding by the measurement restrictions described in Section 5.2.2. On day 32, when the participant's performance meets the condition expressed in (73), the maintenance phase is activated (highlighted in green). This phase reduces reliance on points as incentives to reduce financial dependency, with the allocation of expected and granted points guided by corresponding weights and constraints.

To initiate controller reconfiguration during the intervention's maintenance phase, it is required that *Behavior* remains within a tolerance range of $tol = 400$ steps/day from the target value of 10,000 steps/day for a minimum of 6 out of the last $n_s = 8$ days. The unmeasured disturbance is assumed to follow a Gaussian distribution with a mean of 0 and a standard deviation of 150. On day 40 of the intervention, there is a substantial and sustained drop in temperature (magnitude exaggerated for illustrative purposes) that persists for 8 days. This scenario can be likened to winter cold snap conditions, which often deter individuals from achieving their daily step goals due to significant changes in climate. This disturbance pulse causes a decrease in the participant's step count, pushing it outside of the defined tolerance region. Consequently, the initiation phase is reiterated by the controller. As observed from Fig. 8, the controller reconfiguration facilitates the utilization of financial rewards to incentivize the participant and drive their step count towards the desired level of physical activity (10,000 steps/day), effectively mitigating the effect of the temperature disturbance. Furthermore, the benefits of the disturbance anticipation feature are evident as the controller proactively increases the daily goals provided to the participant one day before the predicted temperature drop (on day 39). This proactive adjustment assists the participant in preparing for the anticipated challenge and encourages them to maintain their step count despite the forthcoming decrease

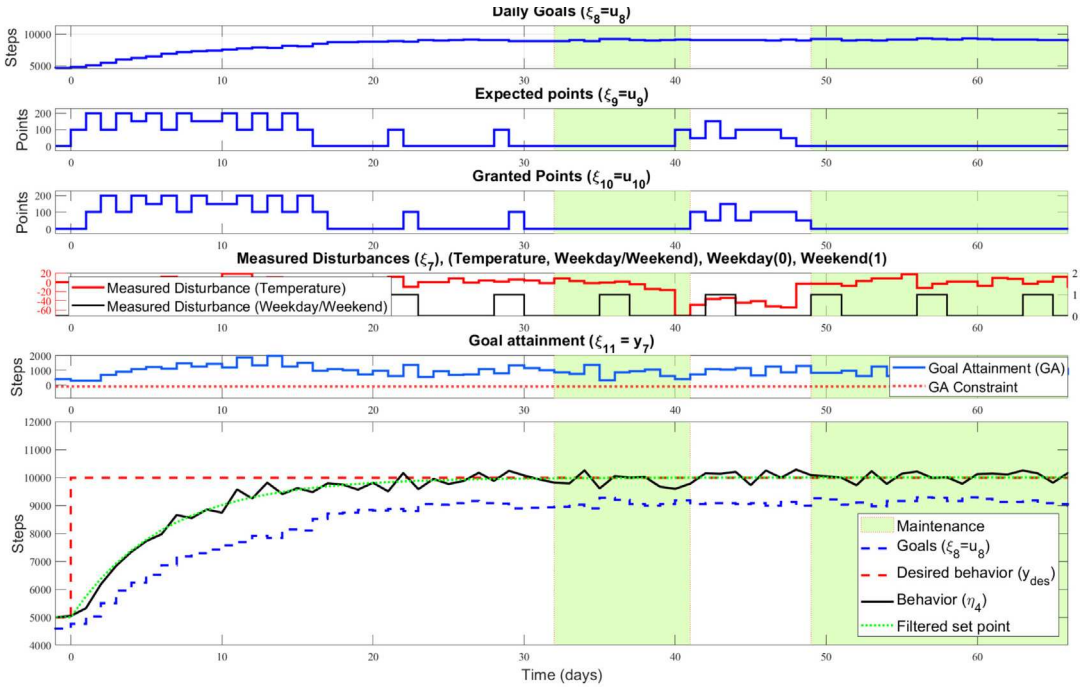

Fig. 8. Simulation results obtained by the application of an HMPC scheme to the *Just Walk* identified ARX model in the presence of both measured (temperature and weekend/weekday) and unmeasured disturbances.

in temperature. As a result, behavior returns to the tolerance region by day 43 of the intervention and stays within this range for the following 6 days. This leads to the subsequent re-activation of the maintenance phase on day 49. Despite the abrupt and high magnitude temperature change, the controller performs well in terms of measured disturbance rejection without violating goal attainment constraints. In addition, as illustrated in Fig. 8, the controller performs well in terms of rejection of stochastic unmeasured disturbance. However, abrupt and very substantial changes in unmeasured disturbances may induce violations of the goal achievement constraint. Hence, the inclusion of slack variables in the objective function (10) is crucial to ensure smooth operation of the controller and prevent infeasibilities that could hinder the implementation of real-world interventions effectively. Throughout the simulation, as depicted in Fig. 8, two types of measured disturbances persist: an autoregressive disturbance characterized by daily temperature changes, and a deterministic disturbance occurring at the start of the weekend. Despite the continuous presence of these disturbances, the controller showcases remarkable ability to reject them and relies on anticipation to accurately maintain the output at the desired setpoint. The anticipation feature proves particularly beneficial when dealing with predictable disturbances like the weekday/weekend signal or when accurate local temperature forecasts are available. The effectiveness of this feature depends directly on the delay of the plant model for a given input. A longer delay enhances the usefulness of the anticipation functionality.

5.3. Application to SIR epidemic model

The purpose of this case study is to demonstrate the effectiveness of the proposed HMPC algorithm on a highly nonlinear system. The *SIR* model is a widely accepted mathematical model for studying the trajectory of epidemics (Rivera et al., 2022; Simon, 2020). It compartmentalizes the overall population into three categories: Susceptible (S), Infected (I), and Recovered (R), and can be visualized as a chemical reactor. In this study, the problem formulation includes births and deaths as inflows and outflows, respectively, thus representing the system as a well-stirred Continuous Stirred Tank Reactor (*CSTR*), as illustrated in Fig. 9. A susceptible person who comes into contact with an infected person is transferred to the infected class. However, the opposite is not true. This mechanism is similar to an irreversible auto-catalytic reaction. Meanwhile, the infected population is removed through recovery or death. These processes can be formulated as a system of chemical reactions:

$$S + I \xrightarrow{\beta(t)} 2I \tag{74}$$

$$I \xrightarrow{\gamma(t)} R \tag{75}$$

$$S \xrightarrow{k_v(t)} R \tag{76}$$

A decrease in $\beta(t)$ implies an increase in social distancing, lockdowns, and masking, and therefore a decrease in $I(t)$. Similarly, assuming a fraction $\gamma(t)$ of the infected population recovers per day, and a fraction μ of the overall population becomes deceased, an increase

Table 2
Control design parameters for *Just Walk* Study.

Parameter	Value	Parameter	Value
p	20 days	$u_{9,max}$	200 points/day
m	10 days	$\Delta u_{8,min}$	$-\infty$
α_d	$[0.5 \quad 0]^T$	$\Delta u_{8,max}$	∞ steps/day
α_r	$[0.85 \quad 0]^T$	$\Delta u_{9,min}$	-100
F_y	diag{0.6, 0}	$\Delta u_{9,max}$	100 points/day
W_y, W_{yt}	diag{1, 0}	y_{min}	$[-\infty \quad -100]^T$
W_u	diag(0, 0.001, 0)	y_{max}	$[\infty \quad \infty]^T$
W_{du}	diag(0.001, 0, 0)	n_s	8 days
$u_{8,min}$	0 steps/day	tol	400 steps
$u_{8,max}$	15 000 steps/day	W_u (maintenance)	diag{0, 1, 0}
$u_{9,min}$	0 points/day	W_s	diag{0, 10}

Table 3
Nominal parameters values for the SIR plant model.

Parameters	Units	Values	Parameters	Units	Values
B_r	Persons/Day	500	$\bar{\beta}$	$\text{Person}^{-1}\text{Day}^{-1}$	0.0005
μ	Day^{-1}	0.2	$\bar{\gamma}$	Day^{-1}	0.29
$\bar{k}_v$	Day^{-1}	0	T_s	Day	1

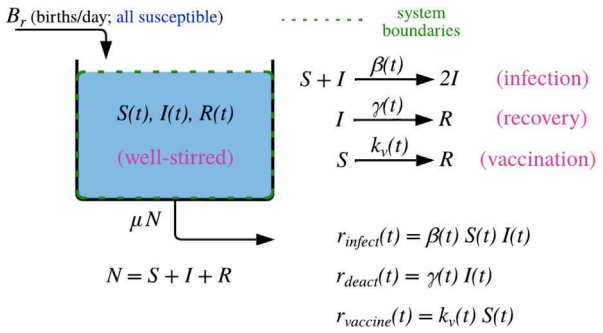

Fig. 9. Schematic illustrating the *SIR* model with births, deaths, and vaccination as a CSTR.
Source: Adapted from Rivera et al. (2022) and Simon (2020).

Table 4
Control design parameters for the *SIR* problem.

Parameter	Value	Parameter	Value
p	50 Days	y_{min}	0
m	20 Days	y_{max}	∞
τ_r	6 Days	Δu_{min}	$-\infty$
τ_d	3 Days	Δu_{max}	∞
τ_u	2 Days	W_y, W_{yt}	1
u_{min}	$0.07\beta_i$	W_{du}(1DoF)	(a) 0.1 (b) 10
u_{max}	∞	W_{du}(3DoF)	0

in $\gamma(t)$ as well as μ causes $I(t)$ to decrease. For this study, μ is held at a fixed value signifying a constant mortality rate. Another factor that affects the system is the fraction of the susceptible population vaccinated per day ($k_v(t)$). An increase in $k_v(t)$ can be instrumental in decreasing $I(t)$ indirectly. Based on these considerations, the use of accounting principles leads to the lumped parameter model:

$$\frac{dS}{dt} = B_r - \beta(t)S(t)I(t) - \mu S(t) - k_v(t)S(t) \tag{77}$$

$$\frac{dI}{dt} = \beta(t)S(t)I(t) - \gamma(t)I(t) - \mu I(t) \tag{78}$$

$$R(t) = \frac{B_r}{\mu} - S(t) - I(t) \tag{79}$$

where B_r denotes the birth rate, $\beta(t)$ is the transmission rate of the infection, $\gamma(t)$ refers to the recovery rate, μ is the mortality rate, and $k_v(t)$ denotes the vaccination rate. $\beta(t)$, $\gamma(t)$, and $k_v(t)$ are time-varying. For constant B_r and μ, the total population $N = \frac{B_r}{\mu} = S(t) + I(t) + R(t)$ remains constant. As noted in Simon (2020), there exist two possible steady states in (77)–(78), where the one resulting in an initial non-zero infected population (i.e., the endemic case) is considered:

$$\bar{S} = \frac{(\mu + \bar{\gamma})}{\bar{\beta}}, \quad \bar{I} = \left(\frac{B_r}{\mu + \bar{\gamma}} - \frac{\mu + \bar{k}_v}{\bar{\beta}}\right) \tag{80}$$

Nominal plant parameters are summarized in Table 3, which are the basis for the linearized model that is provided to the proposed HMPC algorithm (with all E matrices in (4) equal to zero as there are no categorical decisions). The *SIR* model allows us to study the performance of the 3DoF-KF HMPC framework in the presence of disturbances and model uncertainty resulting from linearization. For this purpose, $I(t)$ is considered to be the controlled variable, $\beta(t)$ the manipulated variable, and $k_v(t)$ and $\gamma(t)$ the measured and the unmeasured disturbance, respectively. The controller uses daily sampling ($T_s = 1$ day) with tuning parameters summarized in Table 4.

As depicted in Fig. 10 , a nominal output response that serves as a reference is obtained by simulating the fully unconstrained 3DoF controller on the linearized plant model, as shown by the blue dotted line. This provides an understanding of the workings of the controller in the absence of any plant-model mismatch. For the nonlinear plant model, a comparative study of the proposed framework is done by simulating a traditional single-degree-of-freedom (1DoF) HMPC with move suppression under the same conditions of plant dynamics, input–output constraints, prediction, and move horizons. On day 10, a setpoint change reflecting a 50% reduction in the desired infected population is introduced into the system. Per Fig. 10, the 3DoF-KF HMPC demonstrates a fast closed-loop speed of response in setpoint tracking without any noticeable undershoot or oscillation. To demonstrate disturbance rejection capabilities, a 10% increase in the vaccination rate is introduced at $t = 80$ days. Taking advantage of the increased vaccination rate, the controller increases $\beta(t)$, thus relaxing on lockdown and other social distancing policies that were previously needed to reduce infection. The controller further exhibits robustness and unmeasured disturbance rejection when there is a 10% increase in the recovery rate at day 120. The 3DoF-KF framework accounts for plant-model mismatch and further increases $\beta(t)$ to mitigate it, practically eliminating distancing restrictions and restoring normality. The 3DoF-KF HMPC control, therefore, achieves satisfactory results through physically realizable control actions despite the notable plant-model mismatch and shows a similar output trajectory when compared to the nominal case. In contrast, the move-suppression-based HMPC controller shows evidence of poor epidemic control both in terms of manipulated and control variable responses. For the case of $W_{du} = 0.1$, traditional HMPC displays aggressive control, resulting in underdamped responses. $W_{du} = 10$ detunes the aggressive nature of the controller but still displays significant oscillations and notably long settling times. These indicate the suboptimal performance of 1DoF move-suppression-based control and the superiority of the 3DoF-KF HMPC framework.

6. Summary and conclusions

In this paper, a hybrid model predictive control approach for mixed logical dynamical systems based on Kalman filters is presented, referred to as 3DoF-KF HMPC. The goal is to develop an HMPC-based algorithm that accurately tracks the desired setpoint in the presence of disturbances (measured and unmeasured), nonlinearity, and constraints, relying on discrete and continuous decision-making. The proposed approach provides users with the flexibility of three-degree-of-freedom tuning and incorporates disturbance anticipation. This enables users to independently and intuitively adjust the speed of setpoint tracking and rejection of both measured and unmeasured disturbances. To ensure the optimization problem remains tractable and to address multiple controller objectives with a limited number of manipulated variables, terminal cost, terminal constraint, and slack variables are introduced into the objective function, thereby enhancing its flexibility and adaptability of the algorithm. The effectiveness of the proposed technique was demonstrated by application in three demanding case studies: a production–inventory system, an optimized behavioral intervention based on the *Just Walk* study, and epidemic control demonstrated on the nonlinear SIR model.

As a broad-based algorithm that displays diverse functionality and addresses a myriad of closed-loop requirements, 3DoF-KF HMPC will require a custom implementation in practice; in some settings this will involve software development efforts that while challenging are not insurmountable. For instance, 3DoF-KF HMPC has been applied in an NIH-funded clinical trial (*YourMove*) for increasing physical activity (NIH Reporter, 2020); this effort has involved using MATLAB along with CPLEX optimization software (International Business Machines Corp., 2019), all interfaced with sensor and actuator information in a "glue" layer written in PYTHON. Additional research efforts have been the basis for using 3DoF-KF HMPC to experimentally achieve closed-loop control of *pH* in a pilot-scale raceway bioreactor (Banerjee, Otálora et al., 2024). Enhancements include integration with data-driven "Model-on-Demand" (MoD) estimation for the control of nonlinear, highly-interactive multivariable systems (Banerjee, Khan et al., 2024).

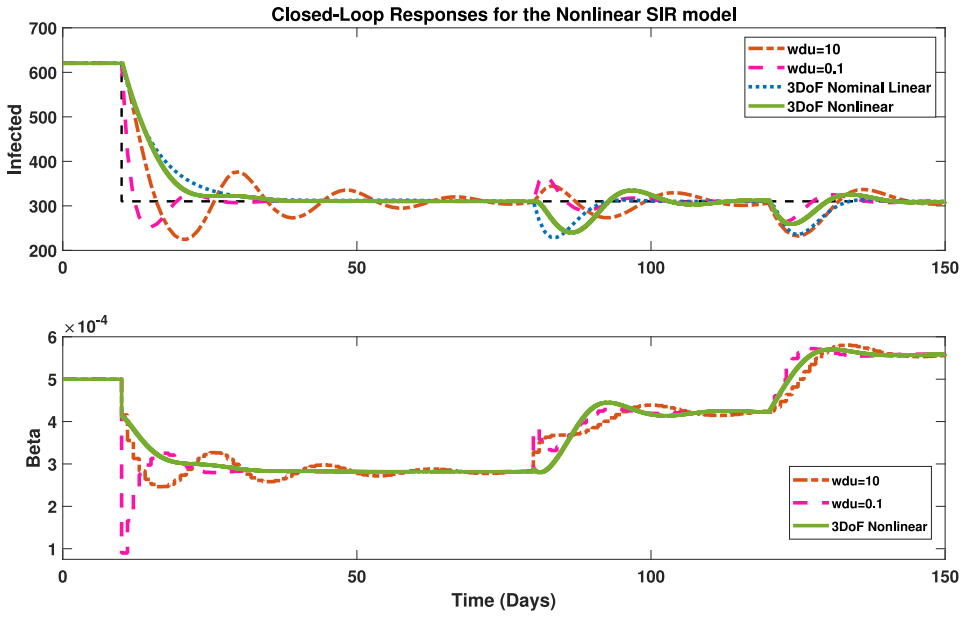

Fig. 10. Evaluation of 3DoF-KF HMPC performance for the *SIR* model with (1DoF) HMPC control. A setpoint change of 50% reduction in the infected population at $t = 10$ days with a step measured disturbance $d_k = 10\%$ increase in vaccination rate at $t = 80$ days and a step unmeasured disturbance $v_k = 10\%$ increase in recovery rate at $t = 120$ days are evaluated for different cases. Case 1 (nominal): The proposed 3DoF controller applied on unconstrained linearized plant (blue, dots), Case 2: the 3DoF formulation applied to the nonlinear *SIR* plant (green, solid), Case 3: 1DoF HMPC with move suppression $W_{du} = 0.1$ (magenta, dashed), Case 4: 1DoF HMPC with move suppression $W_{du} = 10$ (brown, dash-dot). The following constraints were used: $0.07\beta_i \le u_k \le \infty$, and $0 \le y_k \le \infty$. (For interpretation of the references to color in this figure legend, the reader is referred to the web version of this article.)

CRediT authorship contribution statement

Owais Khan: Writing – review & editing, Writing – original draft, Software, Methodology, Investigation, Formal analysis, Conceptualization. **Mohamed El Mistiri:** Writing – review & editing, Writing – original draft, Software, Methodology, Investigation, Conceptualization. **Sarasij Banerjee:** Writing – review & editing, Writing – original draft, Software, Methodology, Investigation. **Eric Hekler:** Writing – review & editing, Resources, Project administration, Investigation, Funding acquisition, Conceptualization. **Daniel E. Rivera:** Writing – review & editing, Writing – original draft, Supervision, Project administration, Methodology, Funding acquisition, Conceptualization.

Declaration of Generative AI in Scientific Writing

While drafting this manuscript, the primary author sought assistance from Grammarly (2024) and ChatGPT (OpenAI, 2023) to improve readability and language. Subsequently, all authors carefully reviewed and edited the text as needed, assuming complete responsibility for the content of the publication.

Declaration of competing interest

The authors declare that they have no known competing financial interests or personal relationships that could have appeared to influence the work reported in this paper.

Acknowledgments

This research was supported by grant R01CA244777 from the National Cancer Institute (NCI) of the National Institutes of Health (NIH), USA and grant 2200161 from the Division of Chemical, Bioengineering, Environmental and Transport Systems (CBET), USA, U.S. National Science Foundation (NSF). The writers' views are their own and may not represent those of NIH and NSF. The authors further appreciate helpful comments and insights from Dr. Naresh N. Nandola of Siemens Corporation and Mr. Francesco Campregher from the University of Brescia, Italy.

Appendix. Matrices associated with the *miqp* problem

The following are the entries for the coefficient matrices described in (50) and (51).

$$\mathcal{Q} = \begin{bmatrix} q_{11} & \mathcal{H}_1{}^T\widehat{W}_y\mathcal{H}_2 & \mathcal{H}_1{}^T\widehat{W}_y\mathcal{H}_3 & 0 \\ \mathcal{H}_2{}^T\widehat{W}_y\mathcal{H}_1 & q_{22} & \mathcal{H}_2{}^T\widehat{W}_y\mathcal{H}_3 & 0 \\ \mathcal{H}_3{}^T\widehat{W}_y\mathcal{H}_1 & \mathcal{H}_3{}^T\widehat{W}_y\mathcal{H}_2 & \mathcal{H}_3{}^T\widehat{W}_y\mathcal{H}_3 + \widehat{W}_z & 0 \\ 0 & 0 & 0 & \widehat{W}_s \end{bmatrix}$$

$$q_{11} = \mathcal{H}_1{}^T\widehat{W}_y\mathcal{H}_1 + R_u^T\widehat{W}_{du}R_u + \widehat{W}_u,$$

$$q_{22} = \mathcal{H}_2{}^T\widehat{W}_y\mathcal{H}_2 + \widehat{W}_d$$

$$\tilde{S}_1 = \begin{bmatrix} \mathcal{E}_1 & \mathcal{E}_2 & \mathcal{E}_3 & 0 \end{bmatrix}, \ \tilde{S}_2 = \begin{bmatrix} \mathcal{H}_1 & \mathcal{H}_2 & \mathcal{H}_3 & -\mathcal{I} \\ -\mathcal{H}_1 & -\mathcal{H}_2 & -\mathcal{H}_3 & -\mathcal{I} \end{bmatrix}$$

$$\tilde{S}_3 = \begin{bmatrix} \mathcal{I} & 0 & 0 & 0 \\ -\mathcal{I} & 0 & 0 & 0 \\ R_u & 0 & 0 & 0 \\ -R_u & 0 & 0 & 0 \end{bmatrix}, \ \tilde{S}_4 = \begin{bmatrix} 0 & 0 & 0 & -\mathcal{I} \end{bmatrix}$$

$$\begin{aligned} g_1 = {} & X_{flt,k}{}^T\Phi^T\widehat{W}_y\mathcal{H}_1 - \mathcal{Y}_{r,flt,k}{}^T\widehat{W}_y\mathcal{H}_1 - \mathcal{U}_{r,k}{}^T\widehat{W}_u - \delta_{k-1}{}^TH_{21}{}^T\widehat{W}_y\mathcal{H}_1 \\ & - u_{k-1}{}^T(R_{u0}{}^T\widehat{W_{du}}R_u + H_{11}{}^T\widehat{W}_y\mathcal{H}_1) - z_{k-1}{}^TH_{31}{}^T\widehat{W}_y\mathcal{H}_1 \\ & - d_{flt,k-1}{}^TH_{d1}{}^T\widehat{W}_y\mathcal{H}_1 + \mathcal{D}_{flt,k}^T\mathcal{H}_d{}^T\widehat{W}_y\mathcal{H}_1 \end{aligned}$$

$$\begin{aligned} g_2 = {} & X_{flt,k}{}^T\Phi^T\widehat{W}_y\mathcal{H}_2 - \mathcal{Y}_{r,flt,k}{}^T\widehat{W}_y\mathcal{H}_2 - \bar{\delta}_{r,k}^T\widehat{W}_d + \mathcal{D}_{flt,k}^T\mathcal{H}_d^T\widehat{W}_y\mathcal{H}_2 \\ & - u_{k-1}^TH_{11}^T\widehat{W}_y\mathcal{H}_2 - \delta_{k-1}{}^TH_{21}{}^T\widehat{W}_y\mathcal{H}_2 - z_{k-1}{}^TH_{31}{}^T\widehat{W}_y\mathcal{H}_2 \\ & - d_{flt,k-1}^TH_{d1}{}^T\widehat{W}_y\mathcal{H}_2 \end{aligned}$$

$$\begin{aligned} g_3 = {} & X_{flt,k}{}^T\Phi^T\widehat{W}_y\mathcal{H}_3 - \mathcal{Y}_{r,flt,k}{}^T\widehat{W}_y\mathcal{H}_3 - \mathcal{Z}_{r,k}{}^T\widehat{W}_z + \mathcal{D}_{flt,k}^T\mathcal{H}_d{}^T\widehat{W}_y\mathcal{H}_3 \\ & - u_{k-1}{}^TH_{11}{}^T\widehat{W}_y\mathcal{H}_3 - \delta_{k-1}{}^TH_{21}{}^T\widehat{W}_y\mathcal{H}_3 - z_{k-1}{}^TH_{31}{}^T\widehat{W}_y\mathcal{H}_3 \\ & - d_{flt,k-1}{}^TH_{d1}{}^T\widehat{W}_y\mathcal{H}_3 \end{aligned}$$

$$\begin{aligned} b_1 = {} & \mathcal{E}_5 - \mathcal{E}_4\hat{X}_k - \mathcal{E}_dD_k + \mathcal{E}_{41}u_{k-1} + \mathcal{E}_{42}\delta_{k-1} + \mathcal{E}_{43}z_{k-1} + \mathcal{E}_{4d}d_{k-1} - \\ & \mathcal{E}_6u_{k-1} - \mathcal{E}_7y_{k-1} + \mathcal{E}_a\bar{a}_k \end{aligned}$$

$$b_2 = \mathcal{Y}_{max} - \Phi\hat{X}_k - \mathcal{H}_dD_k + H_{11}u_{k-1} + H_{21}\delta_{k-1} + H_{31}z_{k-1} + H_{d1}d_{k-1}$$

$$b_3 = -\mathcal{Y}_{min} + \Phi\hat{X}_k + \mathcal{H}_dD_k - H_{11}u_{k-1} - H_{21}\delta_{k-1} - H_{31}z_{k-1} - H_{d1}d_{k-1}$$

$$b_4 = \begin{bmatrix} \mathcal{U}_{max} \\ -\mathcal{U}_{min} \end{bmatrix}, \; b_5 = \begin{bmatrix} R_{u0}u_{k-1} + \Delta\mathcal{U}_{max} \\ -R_{u0}u_{k-1} - \Delta\mathcal{U}_{min} \end{bmatrix}$$

References

Banerjee, S., Khan, O., El Mistiri, M., Nandola, N. N., & Rivera, D. E. (2024). Data-driven control of highly interactive systems using 3DoF Model-on-Demand MPC: Application to a MIMO CSTR. *IFAC-PapersOnLine*, *58*(15), 420–425.

Banerjee, S., Otálora, P., El Mistiri, M., Khan, O., Guzmán, J. L., & Rivera, D. E. (2024). Control-relevant input signal design for integrating processes: Application to a microalgae raceway reactor. *IFAC-PapersOnLine*, *58*(15), 360–365.

Bemporad, A., & Morari, M. (1999). Control of systems integrating logic, dynamics, and constraints. *Automatica*, *35*(3), 407–427.

Berkenkamp, F., & Gwerder, M. (2014). Hybrid model predictive control of stratified thermal storages in buildings. *Energy and Buildings*, *84*, 233–240.

Borrelli, F., Bemporad, A., Fodor, M., & Hrovat, D. (2006). An MPC/Hybrid system approach to traction control. *IEEE Transactions on Control Systems Technology*, *14*(3), 541–552.

Camacho, E. F., Ramírez, D. R., Limón, D., De La Peña, D. M., & Alamo, T. (2010). Model predictive control techniques for hybrid systems. *Annual Reviews in Control*, *34*(1), 21–31.

Deshpande, S., Nandola, N. N., Rivera, D. E., & Younger, J. W. (2014). Optimized treatment of fibromyalgia using system identification and hybrid model predictive control. *Control Engineering Practice*, *33*, 161–173.

El Mistiri, M., Khan, O., Rivera, D. E., & Hekler, E. (2023). System identification and hybrid model predictive control in personalized mhealth interventions for physical activity. In *2023 American Control Conference* ACC, (pp. 2240–2245). IEEE.

Ferrari-Trecate, G., Gallestey, E., Letizia, P., Spedicato, M., Morari, M., & Antoine, M. (2004). Modeling and control of co-generation power plants: A hybrid system approach. *IEEE Transactions on Control Systems Technology*, *12*(5), 694–705.

Gaid, M. M. B., Cela, A., & Hamam, Y. (2006). Optimal integrated control and scheduling of networked control systems with communication constraints: Application to a car suspension system. *IEEE Transactions on Control Systems Technology*, *14*(4), 776–787.

Garcia-Torres, F., Bordons, C., & Ridao, M. A. (2018). Optimal economic schedule for a network of microgrids with hybrid energy storage system using distributed Model Predictive Control. *IEEE Transactions on Industrial Electronics*, *66*(3), 1919–1929.

Garriga, J. L., & Soroush, M. (2010). Model predictive control tuning methods: A review. *Industrial & Engineering Chemistry Research*, *49*, 3505–3515.

Geyer, T., Papafotiou, G., & Morari, M. (2008). Hybrid Model Predictive control of the step-down DC–DC converter. *IEEE Transactions on Control Systems Technology*, *16*(6), 1112–1124.

Grammarly (2024). Grammarly. https://www.grammarly.com.

Groot, N., De Schutter, B., & Hellendoorn, H. (2012). Integrated model predictive traffic and emission control using a piecewise-affine approach. *IEEE Transactions on Intelligent Transportation Systems*, *14*(2), 587–598.

Guo, P., Rivera, D. E., Dong, Y., Deshpande, S., Savage, J. S., Hohman, E. E., Pauley, A. M., Leonard, K. S., & Downs, D. S. (2022). Optimizing Behavioral Interventions to Regulate Gestational Weight Gain With Sequential Decision Policies Using Hybrid Model Predictive Control. *Computers & Chemical Engineering*, *160*, Article 107721.

Hekler, E. B., Rivera, D. E., Martin, C. A., Phatak, S. S., Freigoun, M. T., Korinek, E., Klasnja, P., Adams, M. A., & Buman, M. P. (2018). Tutorial for using control systems engineering to optimize adaptive mobile health interventions. *Journal of Medical Internet Research*, *20*(6), Article e8622.

International Business Machines Corp. (2019). IBM ILOG CPLEX optimization studio: CPLEX 12.10 user's manual. URL https://www.ibm.com/docs/en/icos/12.10.0?topic=cplex-users-manual. [Online; Accessed October 14, 2024].

Khan, O., El Mistiri, M., Rivera, D. E., Martin, C. A., & Hekler, E. (2022). A Kalman filter-based hybrid model predictive control algorithm for mixed logical dynamical systems: Application to optimized interventions for physical activity. In *2022 IEEE 61st Conference on Decision and Control* (pp. 2586–2593). IEEE.

Lee, J. H., Morari, M., & García, C. E. (1994). State-space interpretation of model predictive control. *Automatica*, *30*(4), 707–717.

Lee, J., & Yu, Z. (1994). Tuning of model predictive controllers for robust performance. *Computers & Chemical Engineering*, *18*(1), 15–37.

Maciejowski, J. M. (2002). *Predictive Control with Constraints*. London, UK: Pearson Education.

Martín, C. A., Rivera, D. E., & Hekler, E. B. (2016). A decision framework for an adaptive behavioral intervention for physical activity using Hybrid Model Predictive Control. In *2016 American Control Conference* (pp. 3576–3581). IEEE.

Martín, C. A., Rivera, D. E., Hekler, E. B., Riley, W. T., Buman, M. P., Adams, M. A., & Magann, A. B. (2020). Development of a control-oriented model of Social Cognitive Theory for optimized mhealth behavioral interventions. *IEEE Transactions on Control Systems Technology*, *28*(2), 331–346.

Morari, M., & Zafiriou, E. (1989). *Robust Process Control*. Englewood Cliffs, NJ: Prentice-Hall.

Nandola, N. N., & Rivera, D. E. (2013). An improved formulation of hybrid Model Predictive Control with application to production-inventory systems. *IEEE Transactions on Control Systems Technology*, *21*(1), 121–135.

NIH Reporter (2020). *Optimizing Individualized and Adaptive mHealth Interventions via Control Systems Engineering Methods*. R01CA244777: National Institute of Health, National Cancer Institute, URL https://reporter.nih.gov/search/g7QkpEP3VUS-bXgSgfT-GA/project-details/10051197.

OpenAI (2023). ChatGPT. https://chat.openai.com.

Phatak, S. S., Freigoun, M. T., Martín, C. A., Rivera, D. E., Korinek, E. V., Adams, M. A., Buman, M. P., Klasnja, P., & Hekler, E. B. (2018). Modeling individual differences: A case study of the application of system identification for personalizing a physical activity intervention. *Journal of Biomedical Informatics*, *79*, 82–97.

Rivera, D. E., El Mistiri, M., & Shi, Z. (2022). Using SIR epidemic modeling and control to teach process dynamics and control to chemical engineers. *IFAC-PapersOnLine*, *55*(17), 380–385.

Rossiter, J. (2003). *Model-Based Predictive Control: A Practical Approach*. Boca Raton, FL: CRC Press.

Schwartz, J. D., & Rivera, D. (2010). A process control approach to tactical inventory management in production-inventory systems. *International Journal of Production Economics*, *125*(1), 111–124.

Schwartz, J. D., Wang, W., & Rivera, D. E. (2006). Simulation-based optimization of process control policies for inventory management in supply chains. *Automatica*, *42*(8), 1311–1320.

Simon, C. M. (2020). The SIR dynamic model of infectious disease transmission and its analogy with chemical kinetics. *PeerJ Physical Chemistry*, *2*, Article e14.

Timms, K. P., Rivera, D. E., Piper, M. E., & Collins, L. M. (2014). A hybrid model predictive control strategy for optimizing a smoking cessation intervention. In *2014 American Control Conference* (pp. 2389–2394). IEEE.

Torrisi, F. D., & Bemporad, A. (2004). HYSDEL–A tool for generating computational hybrid models for analysis and synthesis problems. *IEEE Transactions on Control Systems Technology*, *12*(2), 235–249.

Williams, H. (1993). *Model Building in Mathematical Programming*. John Wiley & Sons, New York.

Zhou, K., Doyle, J. C., & Glover, K. (1996). *Robust and Optimal Control*. New Jersey: PTR Prentice Hall.

Owais Khan Owais Khan received the B.Sc. degree in electronics engineering from University of Engineering and Technology (UET) Peshawar, Pakistan, in 2011, the M.S. degree in electrical engineering with specialization in control systems from COMSATS University, Islamabad, Pakistan, in 2016, and the Ph.D. degree in electrical engineering with specialization in control systems from the Pakistan Institute of Engineering and Applied Sciences (PIEAS), Islamabad, in 2020. He is currently working as a Postdoctoral Research Scholar at the Control Systems Engineering Lab, Arizona State University, USA. His research interests include model predictive control, fault tolerant control, state estimation, optimization, system identification and the application of control system theory to different dynamical systems related to (but not limited to) robotics, chemical processes, and behavioral medicine.

Mohamed El Mistiri Mohamed El Mistiri received the B.S. degree in Chemical Engineering from Arizona State University (ASU), in 2017, the M.S. degree in Chemical Engineering from ASU, in 2023, and the Ph.D. degree in Chemical Engineering with a focus on Control Systems, in 2024. He is currently a Postdoctoral Research Scholar at the Control Systems Engineering Lab, ASU. His research interests include control theory, system identification, dynamic modeling, and optimization in process systems, robotics, supply chain management, and healthcare.

Sarasij Banerjee Sarasij Banerjee is a PhD candidate at Arizona State University in the Control Systems Engineering Lab. He received his B.Tech. in Chemical Engineering from the Indian Institute of Technology Kanpur (IITK) in 2021. His work focuses on system identification, control theory, and optimization with applications to healthcare, sustainability, and chemical engineering.

Eric Hekler Eric Hekler received the Ph.D. in Clinical Health Psychology from Rutgers University and completed postdoctoral training at Stanford University. He is Professor in the Herbert Wertheim School of Public Health and Human Longevity Sciences (HWSPH). Eric is a transdisciplinary researcher, educator, and practitioner who works at the intersection of public health (primary affiliation), health psychology (original training), design, and systems science. His mission is to advance methods and processes that equitably serve people and practice towards a more vital, just, and resonantly diverse society and planet. He is recognized internationally as an expert in applied health science methods and digital health.

Daniel E. Rivera Daniel E. Rivera received the B.S. degree in chemical engineering from the University of Rochester, Rochester, NY, USA, in 1982, the M.S. degree in chemical engineering from the University of Wisconsin–Madison, Madison, WI, USA, in 1984, and the Ph.D. degree in chemical engineering from the California Institute of Technology, Pasadena, CA, USA, in 1987. From 1987–1990, he was a member of the Control Systems Section, Shell Development Company, Houston, TX, USA. He joined Arizona State University, Tempe, AZ, USA in 1990 and is currently Professor of chemical engineering with the School for Engineering of Matter, Transport, and Energy in the Ira A. Fulton Schools of Engineering. His research interests include system identification, robust process control, and applications of control engineering to problems in supply chain management and behavioral medicine.